Modal Testing Repeatability of a Population of Spherical Shells

Los Alamos
NATIONAL LABORATORY

Edited by Karen Sharkey, Group IM-1

Modal Testing Repeatability of a Population of Spherical Shells

A. Robertson*

F. Hemez

I. Salazar

T. Duffey

*Consulting Engineer, HYTEC, Inc., 4735 Walnut, Suite W-100, Boulder, CO 80305

Los Alamos
NATIONAL LABORATORY

Contents

Modal Testing Repeatability of a Population of Spherical Shells

by

A. Robertson, F. Hemez, I. Salazar, and T. Duffy

Abstract

In this study, we investigated the variability in modal frequencies obtained from testing a set of hollow, almost spherical marine floats. We investigated four sources of variability: unit-to-unit variability, operator-to-operator variability, test repetition, and accelerometer placement. Because we measured the excitation and response of the marine floats, we were able to estimate impulse response and frequency response functions. Variability is assessed by measuring the deviation of each frequency response function from the mean curve for its test group. We ranked unit-to-unit variability the highest, followed by accelerometer placement, operator-to-operator, and test-to-test. We performed analyses of the correlation between temporal and spectral moments extracted from the time responses, impulse responses, auto-spectral densities, and frequency response functions. We completed the study with a principal component analysis and ARMAX modeling. With the exception of ARMAX modeling, all analysis techniques led to the same conclusion. We used an automated eigen extraction technique, the Eigensystem Realization Algorithm, to study the variability of resonant frequencies and modal damping ratios. We also investigated the effects of mass and geometry on variability. We found a strong correlation between the frequency and mass for the fundamental mode only. Our comparison between the measured frequencies and analytical values obtained from a purely spherical shell theory indicates that the floats are indeed very close to spherical. Our main conclusion is that the majority of analysis techniques find the unit-to-unit variability to be the largest by a significant margin; the second largest is the variability caused by accelerometer placement, followed by the operator-to-operator variability and test-to-test variability.

_____

1.   Executive Summary

In this study, we investigated the variability in modal frequencies obtained from testing a set of hollow, almost spherical marine floats. We focused on four sources of variability: unit-to-unit variability (U2U), operator-to-operator variability (020), test repetition (T2T), and accelerometer placement (Acc). For the Acc, the test setup had to be reconfigured, thereby encompassing the T2T variability as well. Of course, U2U tests require a new test setup and Acc for each test performed, so it should encompass the variability of both T2T and Acc. A summary of the tests performed is given in Table 1.

A more thorough description of the test articles and sources of variability are given in Section 2, and an explanation of the modal test setup and equipment is given in Section 3. The experimental procedure for the modal test is summarized in Section 4. Each test measured both the excitation and response of the float, from which impulse response functions (IR) and their corresponding frequency response functions (FRF) were calculated. We used all of these functions, with the exception of the input, to assess the variation between the different data sets. Section 4 also summarizes two other sets of tests that were performed: a high-bandwidth test to look at higher frequency modes, and a set of noise tests to assess the noise level in the data.

Section 5 presents the results of the testing and encompasses the majority of this report. In Section 5.1, we present the results of the noise tests, which are summarized in Table 2. Section 5.2 displays the FRF plots for all of the tests for the response from accelerometer 2. You can easily assess the variability within each group of tests performed. We estimated this variability by measuring the deviation of each FRF from the mean FRF for its test group (see Figure 25). This plot shows the first assessment of which source provides the highest variability. U2U variability appears to be the highest, then Acc and O2O, with T2T being the lowest. As mentioned before, Acc should be higher than T2T, since it encompasses the T2T variability as well.

In Section 5.3.1, which discusses the correlation between the responses, we used the IRs, the auto spectral densities, and the FRFs within each test group to show the variability in the data (see Figure 26 and Figure 27). This approach, however, involves using highly dimensional data. To reduce the dimensionality of the data, we extracted features that would represent the important characteristics of each data set. We examined three different types of features: temporal and spectral moments in Section 5.3.2 (see Figure 28 and Figure 29), principal component analysis in Section 5.3.3 (see Figure 31 and Figure 34), and ARMAX modeling in Section 5.3.4 (see Figure 35 and Figure 36). With the exception of ARMAX modeling, all features, including the correlation, produced the same conclusion: U2U variability is the highest by far, with Acc or O2O coming in second, and T2T being the lowest. In some cases T2T does not differ greatly from Acc and O2O, all three having fairly low variability.

The preceding conclusion is partly supported by the results of an analysis of the variability in the extracted modes themselves. In Section 5.4, we used an eigensystem realization algorithm (ERA) to extract the first four modes from each of the tests. The first mode showed more change in frequency caused by T2T over Acc, which violates our previous assumptions (see Figure 42). This is not true in the other three modes, though for these, Acc variability appears to be as large, or larger, than the U2U variability.

In the investigation of the four sources of variability, we used only one float in the tests, with the exception of the U2U tests. Some of the variation in the frequencies could also be caused by differences in the mass of the floats. Section 5.5 looks at the correlation between the mass of the floats and the frequencies. Only mode 1 showed a strong correlation between mass and frequency (see Figure 43). We assumed, therefore, that variations in the geometry are more important than small mass changes for the other three modes.

Finally, Section 6 presents a method for extracting the analytical frequencies of purely spherical, hollow shells. We compared these frequencies to the experimental values in Table 6 through Table 9, and found that they corresponded well. This means that the floats are indeed very close to spherical.

Our conclusions are given in the final section, Section 7. Our main conclusion is that the majority of analysis techniques find U2U variability in the testing to be the largest by a significant margin. The second largest is the variability caused by Acc. Next is the O2O variability, with T2T variability being about the same.

2. Introduction

The purpose of this study was to quantify sources of variability in the modal response of a population of "identical" marine floats. The primary sources of variability for this study were the following:

- **Unit-to-unit variability (U2U):** Variation from conducting the same test on each float in the population.

- **Test-to-test variability (T2T):** Variation from one modal test being repeated on the same float.

- **Operator-to-operator variability (O2O):** Variation from different operators performing the same modal test and data analysis on the same float.

The test components are "off-the-shelf," commercially available marine floats (see Figure 1) commonly used by the petrochemical industries in large open or closed tanks for liquid level (gage) measurements [1,2,3]. The marine floats were purchased directly from Quality Float Works in Schaumburg, Illinois [4]. Each float has a 9-inch outside diameter, 16-gage shell thickness, and no optional external piping connections. Marine floats are made from Type 304L stainless steel in two hemispheres that are welded together. The float also has a weld at the top, sealing it from outside air.
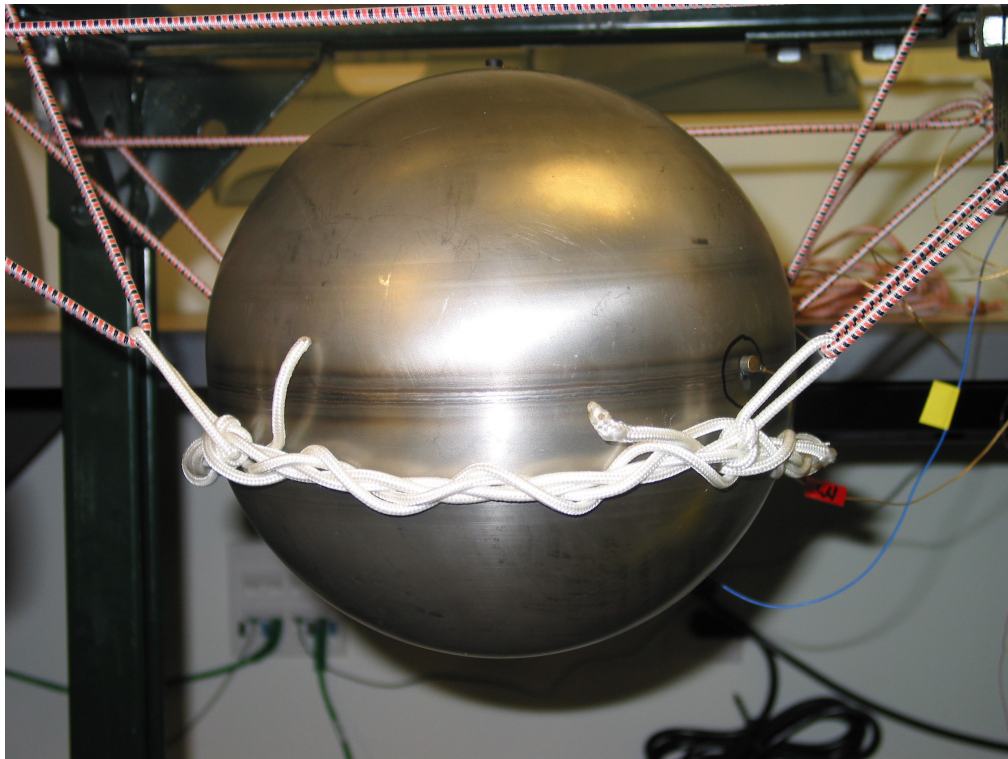
Figure 1: Marine float hanging in test apparatus.

The main motivation for the study was to understand the natural variability when performing simple tests in a well-controlled environment. Understanding the variability and quantifying where it comes from is important for the development of numerical models that predict the structural response of spherical geometries. Although the analytical and numerical modeling of spheres has been extensively studied in the literature, little information is available on the degree of variability that can be expected from a lot of nominally identical, manufactured spheres. Clearly, such variability needs to be known to guide the level of accuracy of numerical models.

3.   Experimental Configuration

The test apparatus consisted of a braided rope ring supported by four points on a three-legged frame with elastic cord, as shown in Figure 2. (Figure 3 shows a close-up of the apparatus.)
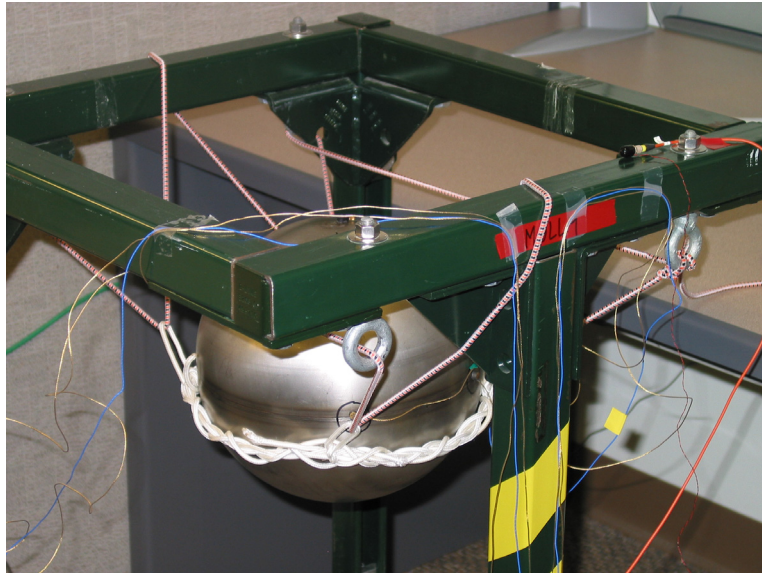
Figure 2: Modal float test apparatus.

We placed each float into the rope ring with the equatorial weld horizontal and the polar weld facing up. We used three accelerometers for the testing, and placed them on each float in the same orientation for each test. Channel 2 of the data acquisition was for the accelerometer placed near the polar weld and Channels 3 and 4 were for the accelerometers placed on the equator from left to right respectively, as shown in Figure 4.
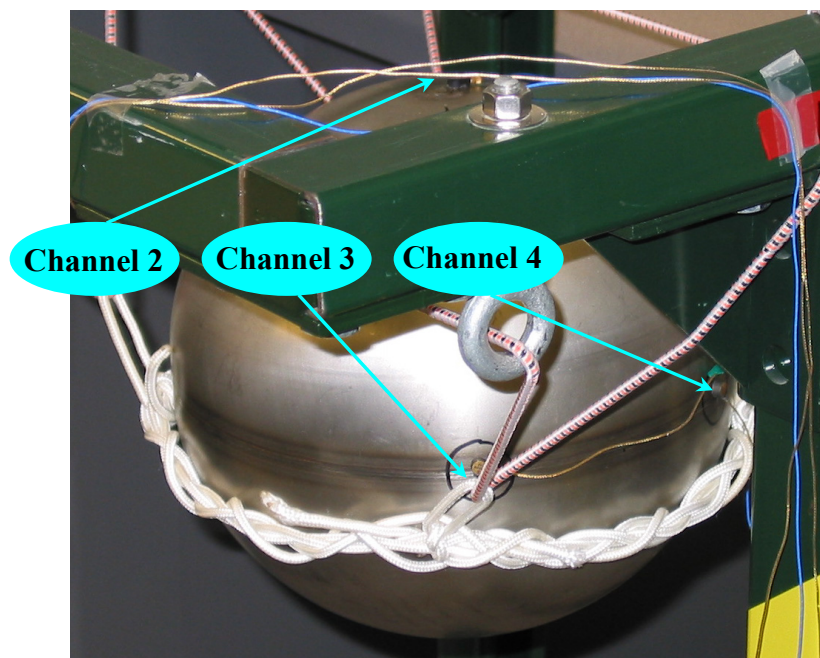
Figure 3: Close-up picture of float and accelerometer placement.
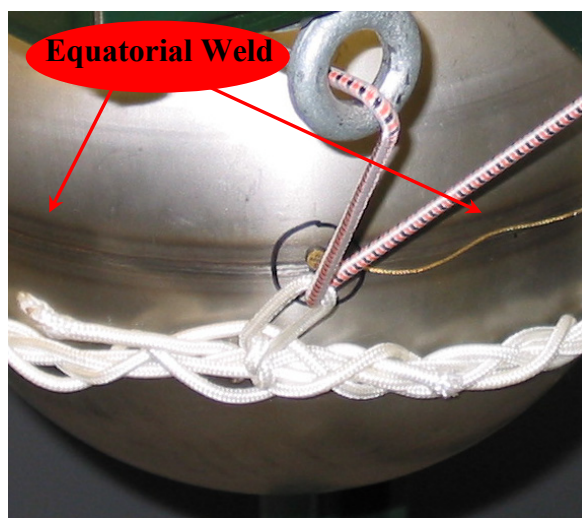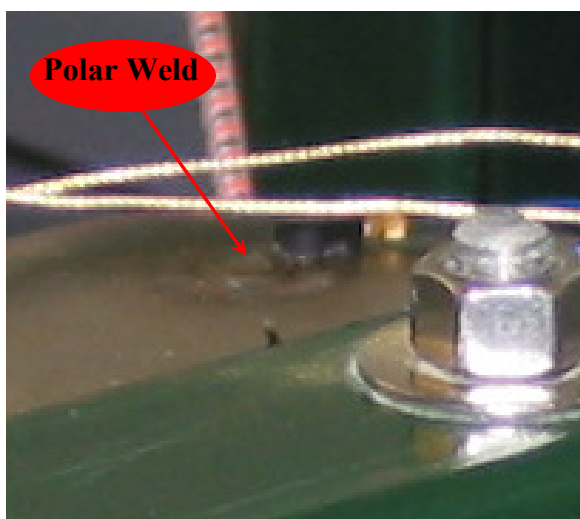
Figure 4: Polar and equatorial welds identified.

4.   Experimental Procedure

We instrumented each float with accelerometers and inserted them into the test apparatus in a similar manner. We used three accelerometers to measure the modal response: two accelerometers were placed sixty degrees apart on the equator, and a third accelerometer was placed on the pole beside the weld. We used a small impact hammer, shown in Figure 5, to excite the high-frequency modes of the float.

Figure 5: Excitation hammer from PCB piezotronics.

We marked the excitation point on the float at forty-five degrees from the polar axis away from the accelerometers placed on the equator weld. Figure 6 shows the excitation point being impacted with the impact hammer.
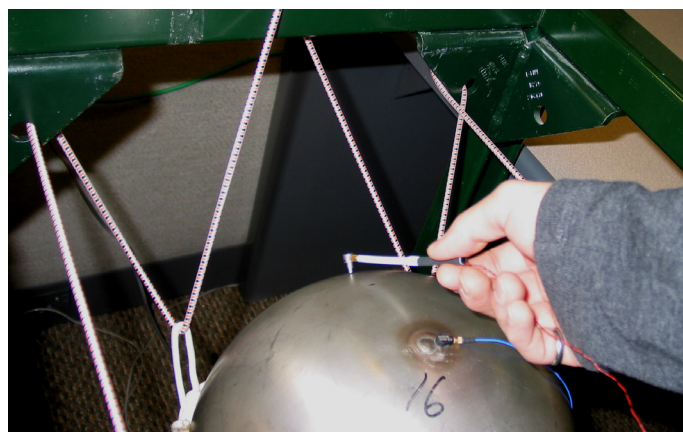
Figure 6: Impact location.

We recorded a measurement of both the input force and the output acceleration at the three accelerometer locations for each test. The sampling frequency was 20,480 Hz, with a data-block size of 4,096. We used a Dactron data-acquisition system, which performs antialiasing on the data and averaging in the frequency domain. The number of averages for each data set was equal to ten. More information on the settings for the data-acquisition system can be found in Appendix A.

Table 1 summarizes the tests performed, and details are provided in Sections 4.1 to 4.5 below.

Table 1: Summary of the modal tests performed.

Type of Test	Number of Averages	Number of Replicates	Bandwidth	Number of the Float Used
U2U	10	14	0-10.24 kHz	All 14 floats
T2T	10	10	0-10.24 kHz	16
Acc	10	10	0-10.24 kHz	16
O2O	10	4	0-10.24 kHz	16
High Bandwidth	10	5	0-24.00 kHz	16,17,18,19,20
Noise	10	5	0-10.24 kHz	16

4.1   Unit-to-Unit (U2U) Variability

We carefully tested the population of fourteen floats using the same procedure to quantify the U2U variability. Each of the fourteen floats was instrumented with accelerometers and placed in the rope ring for testing. Each U2U variability data set consists of fourteen replicates, one for each float, and each replicate consists of ten averaged runs. Once we obtained data for all fourteen floats, we chose a nominal float (number 16), and conducted three sets of tests: two T2T variability tests, and the O2O variability test.

4.2   Test-to-Test (T2T) Variability

The first T2T test we conducted was the suspension system variability test. Here the float was removed from the wire rope and carefully replaced with the equatorial weld oriented as close to horizontal as possible for each test. Each T2T variability data set consists of ten replicates with each replicate consisting of ten averaged runs.

We used the second T2T test to observe the sensitivity of Acc on the equatorial weld. The accelerometers were slightly misplaced and the test was repeated. Because the float needed to be removed from the rope ring, variability obtained from the suspension system placement was included in the Acc variability test. We used the first eight tests to change the two accelerometers placed on the equator, and the last two tests examined the effect of the placement of the accelerometer on the pole. Table 14 in Appendix B lists the particular Accs for each test.

4.3   Operator-to-Operator (O2O) Variability

Finally, we considered O2O variability by repeating the same test with four different operators. Each O2O variability data set consists of four replicates with each replicate consisting of ten averaged runs. We left the float in the same position for each O2O test, and the accelerometers remained in the same configuration.

4.4   High-Bandwidth Test

For a more complete comparison to analytical data, we needed to identify more high-frequency modes. We conducted the high-bandwidth test to identify modes up to 21,000 Hz by using a sampling rate of 48,000 Hz. We conducted five replicates, with each containing ten averaged runs. We used float numbers 16, 17, 18, 19, and 20 for the high-bandwidth test. After each test, the float was removed from the suspension system and accelerometers were placed on the next float, which was then suspended.

4.5   Noise Tests

We investigated the amount of isolation in the frame/elastic-mounting device by using the tests entitled "noise tests." We performed these five tests with the Channel 2 accelerometer at an arbitrary point on the float, Channel 3 halfway up the yellow leg, and Channel 4 on the upper square tube near the eyelet (see Figure 7). The tests determined the amount of isolation the float had while seated in the suspension system. We chose float number 16 for the noise tests. Test numbers 1, 4, and 5 were free run tests, based on ambient excitation sources solely, while tests 2 and 3 were the average of ten impacts on the legs.
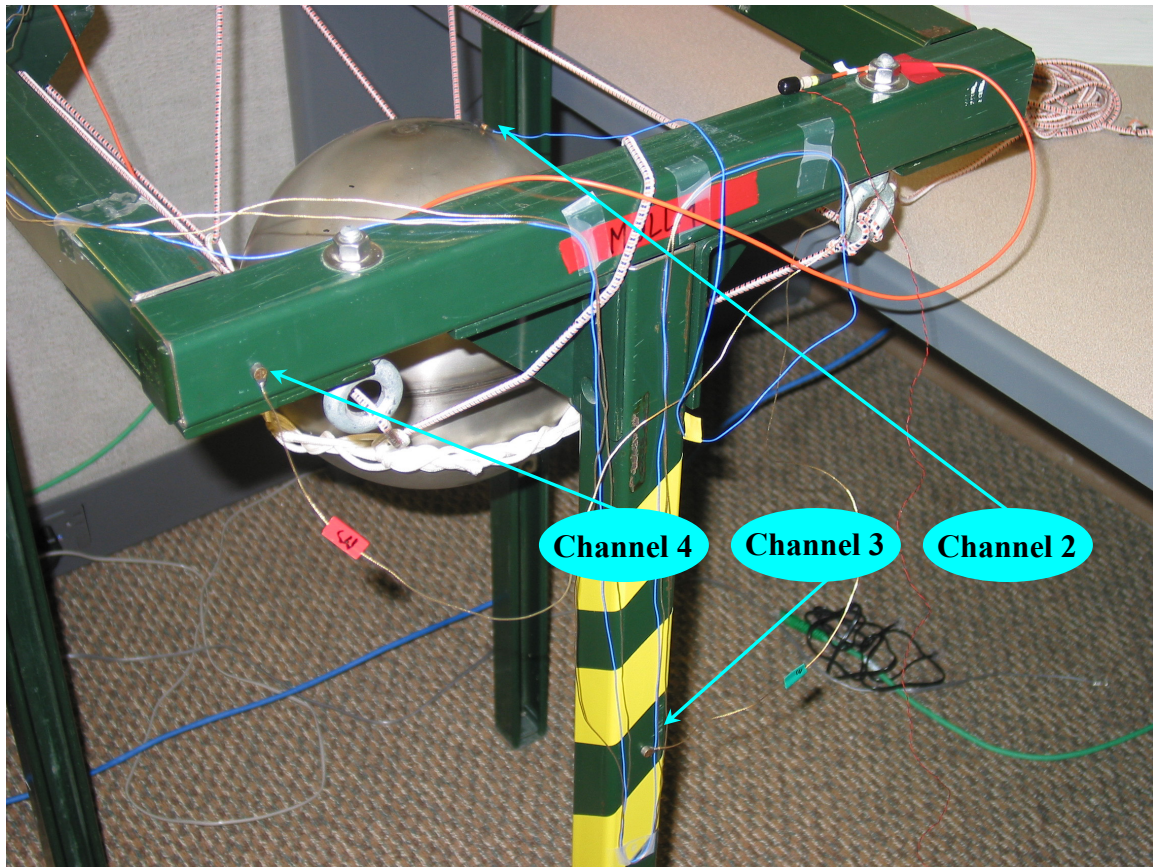

Figure 7: Measurement points for the noise tests.

5.   Results

We present five different sets of results in this section: noise test data, FRF data, feature extraction, ERA fit, and mass correlation. We used these results to assess the amount of variation present in the data caused by the different testing situations presented above.

5.1   Noise Tests

The noise tests are summarized as follows (refer to Figure 7 for a picture of the test setup). The first test had no excitation and measured the background noise present. The second noise measurement was the result of an impact on the leg with yellow tape. The third noise measurement was the result of an impact on one of the green legs. Both excitation points were near the bottom of the frame's legs, near the floor. Results of the noise test are presented in tabular form (Table 2) showing the standard deviation of the acceleration-time history for comparison. The standard deviation of the noise signals is much smaller when compared to the other tests performed.

Table 2: Noise test results (standard deviation of acceleration [g] time history).

	Channel 2 (On Float)	Channel 3 (Half Up Yellow Leg)	Channel 4 (Near eyelet)
Noise 1 (Background Noise)	0.023	0.037	0.036
Noise 2 (Impact on Yellow Leg)	0.089	12.63	4.625
Noise 3 (Impact on Green Leg)	0.066	1.330	2.589
Noise 4 (Free Run, Stomping on Floor)	0.024	0.036	0.036
Noise 5 (Free Run, No Stomping)	0.023	0.036	0.035

5.2   Frequency Response Data (Channel 2)

In this section, we present the plots of all the FRF and their mean, plus or minus one standard deviation, for each test (see Appendix C for the definition of the FRF). Also shown are the coherence measurements for each data set. Data collected from the Channel 2 accelerometer (see Figure 8) are the signals examined in the following figures because they exhibit the cleanest plots (lowest noise-to-signal ratios) with the most distinct mode peaks.
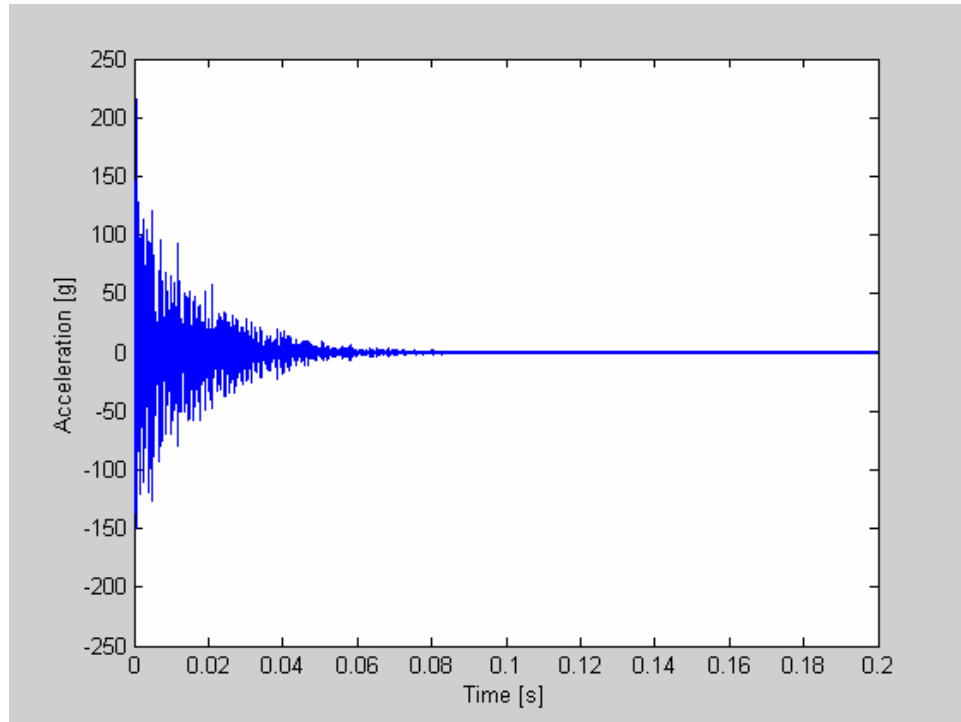
Figure 8: Sample acceleration time history.
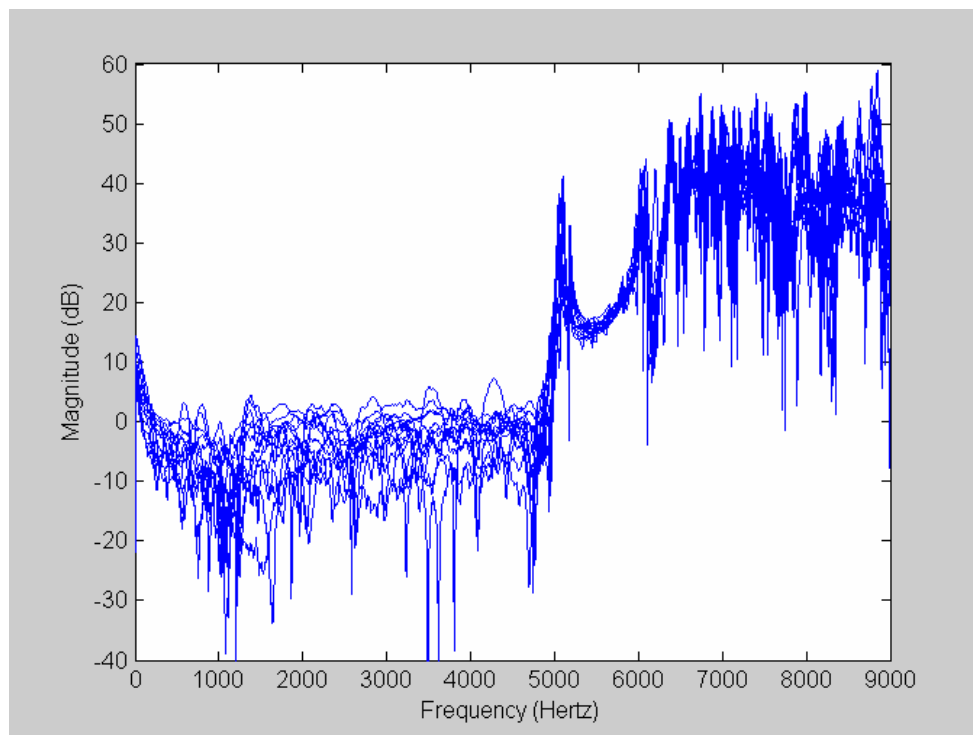
Figure 9: U2U tests, FRF21. (All data sets collected.)

Figure 10: U2U tests, FRF21. (Mean and mean +/- one standard deviation.)
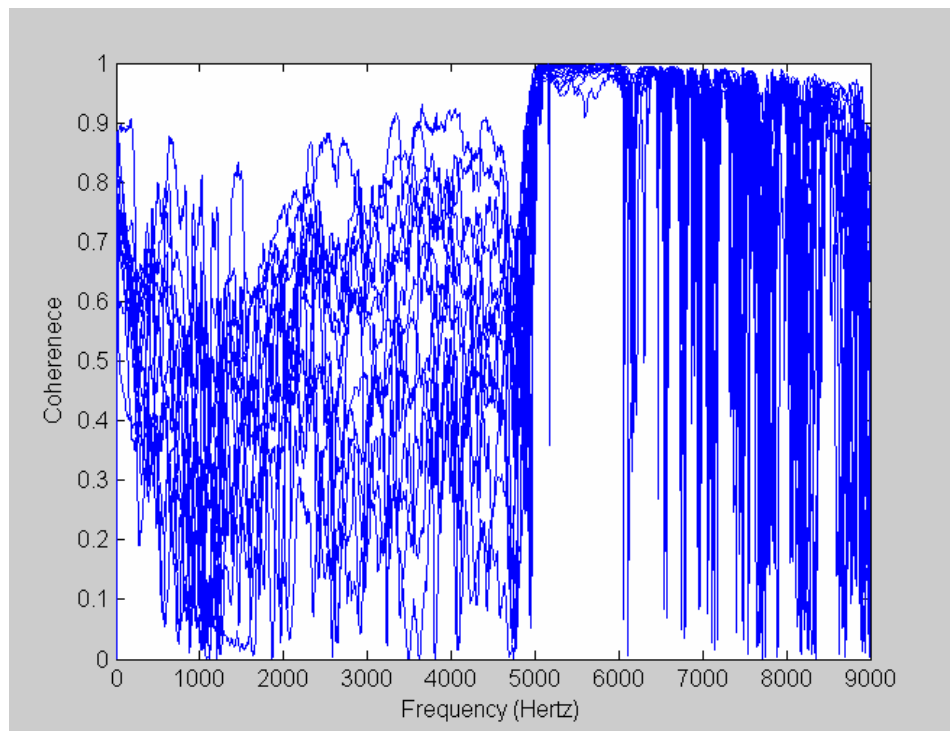
Figure 11: U2U coherence, FRF21. (All data sets collected.)
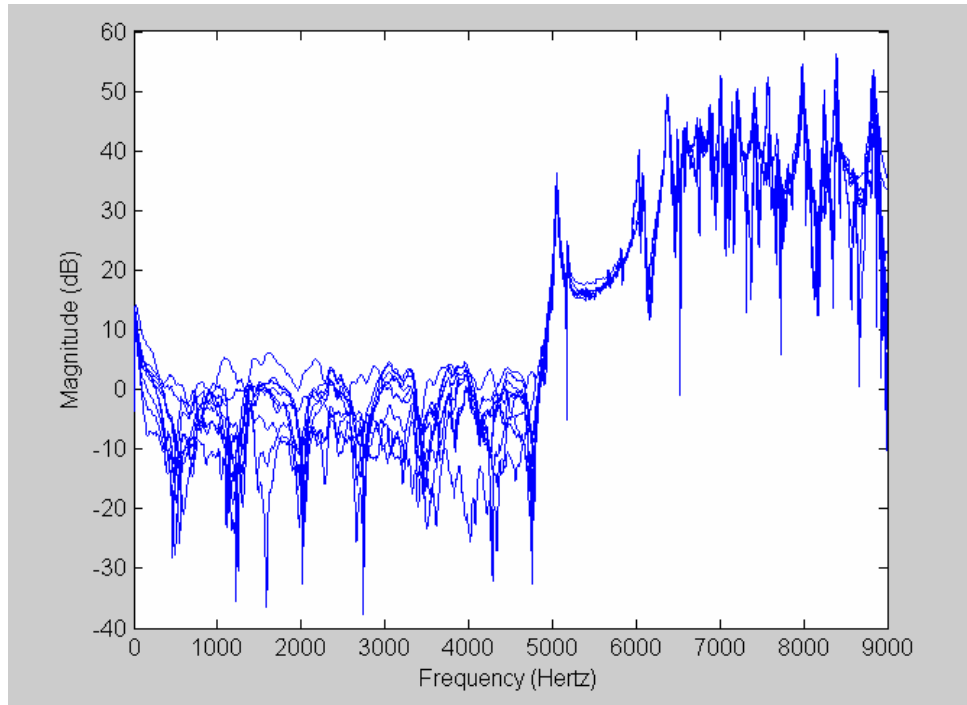
Figure 12: Acc tests, FRF21. (All data sets collected.)
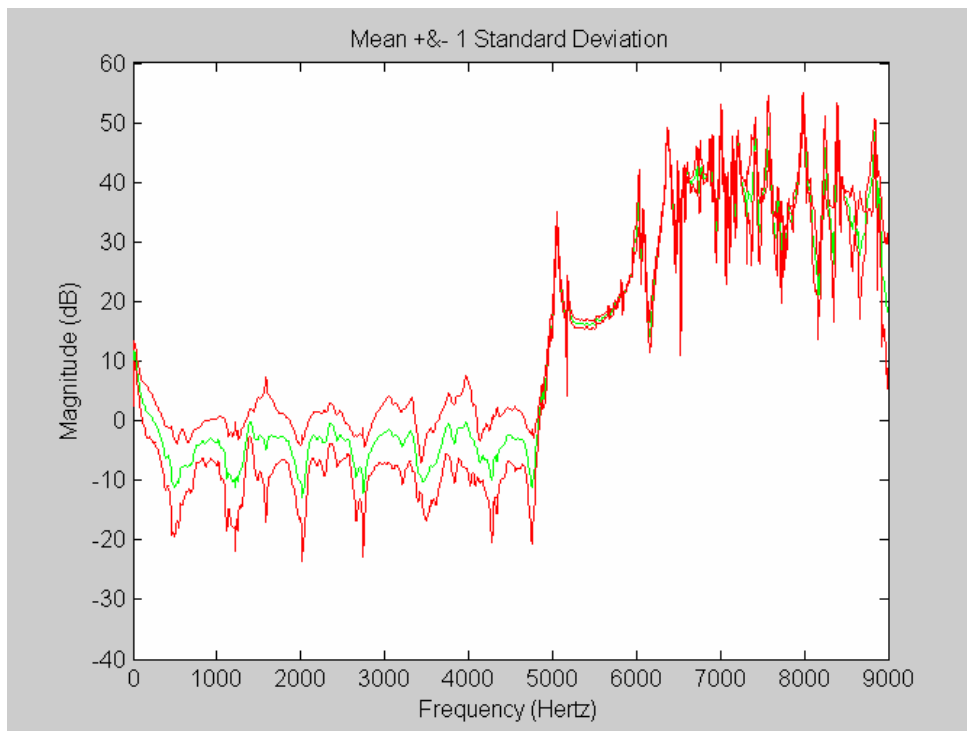
Figure 13: Acc tests, FRF21. (Mean and mean +/- one standard deviation.)
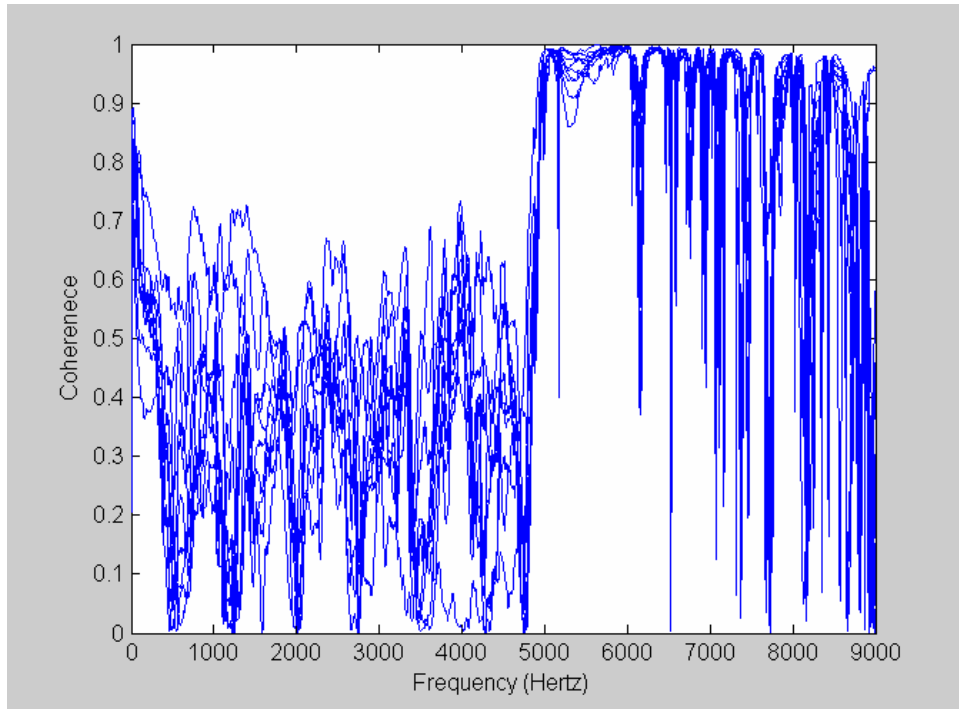
Figure 14: Acc coherence, FRF21. (All data sets collected.)
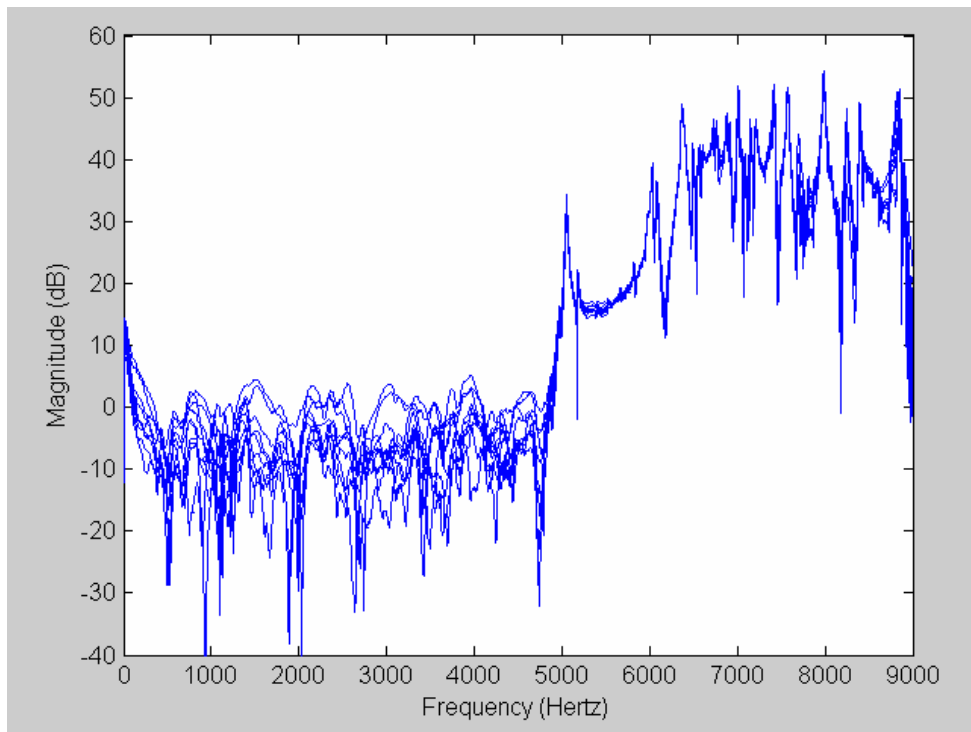
Figure 15: Suspension system (T2T) tests, FRF21. (All data sets collected.)
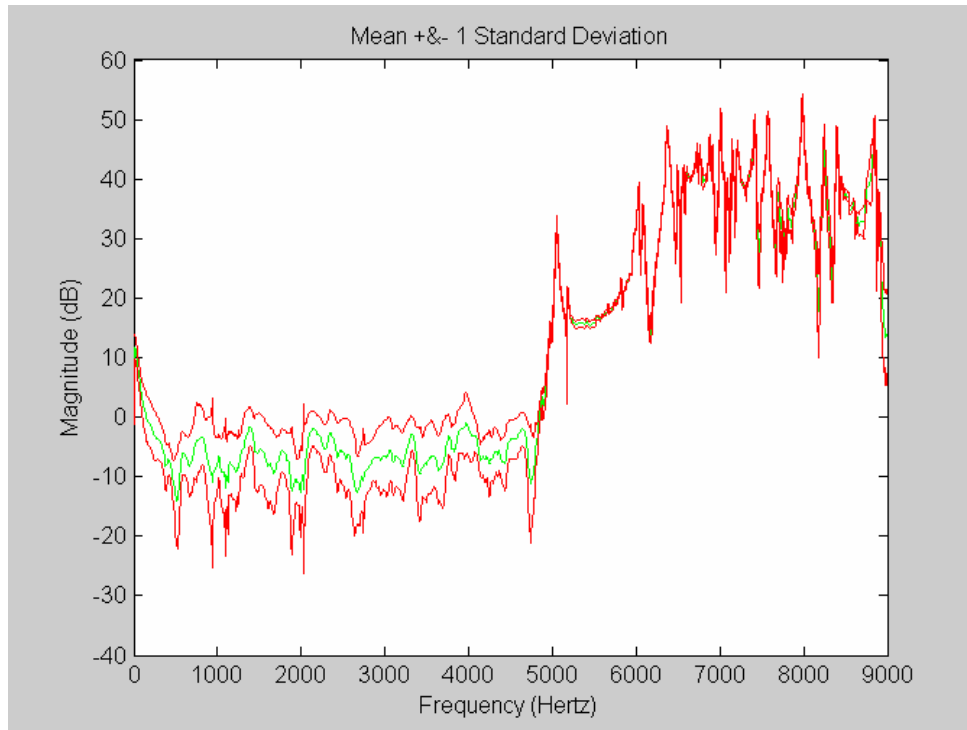
Figure 16: Suspension system tests, FRF21. (Mean and mean +/- one standard deviation.)
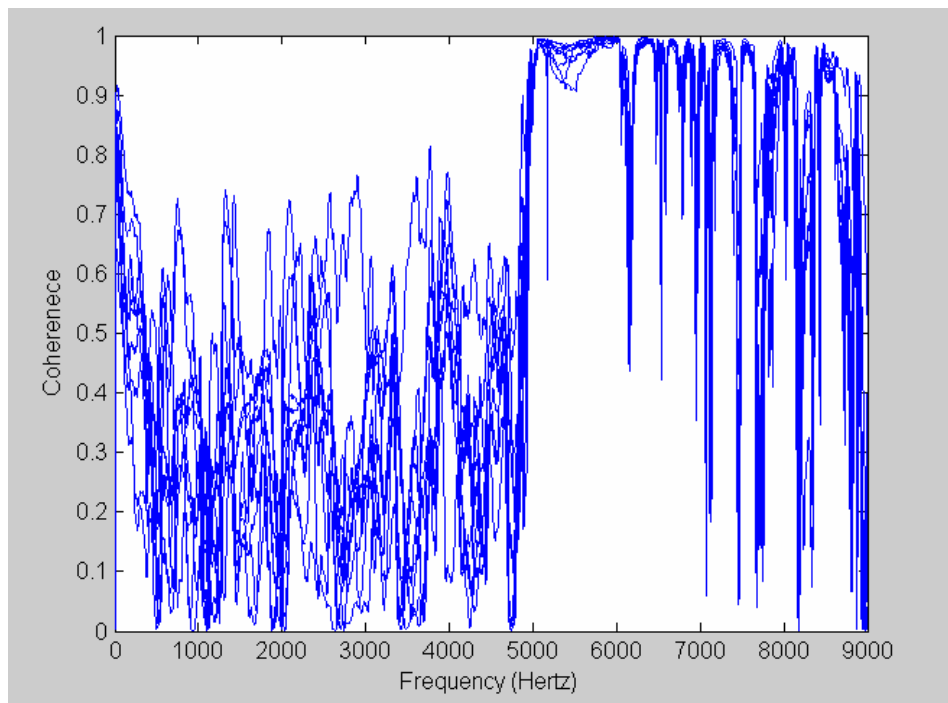
Figure 17: Suspension system coherence, FRF21. (All data sets collected.)
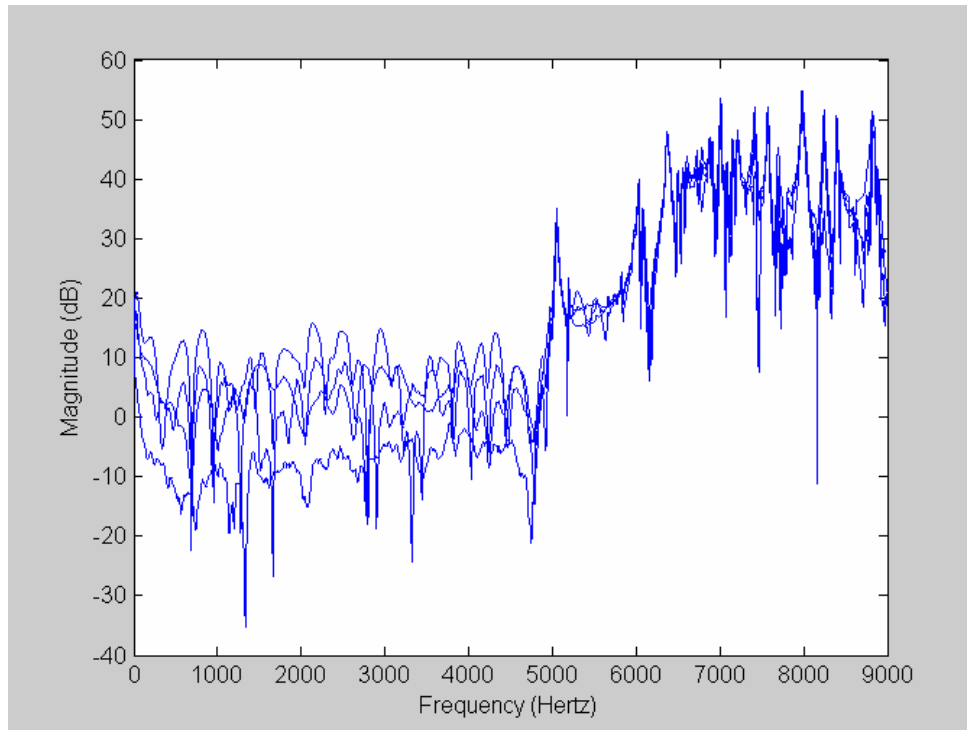
Figure 18: O2O tests, FRF21. (All data sets collected.)
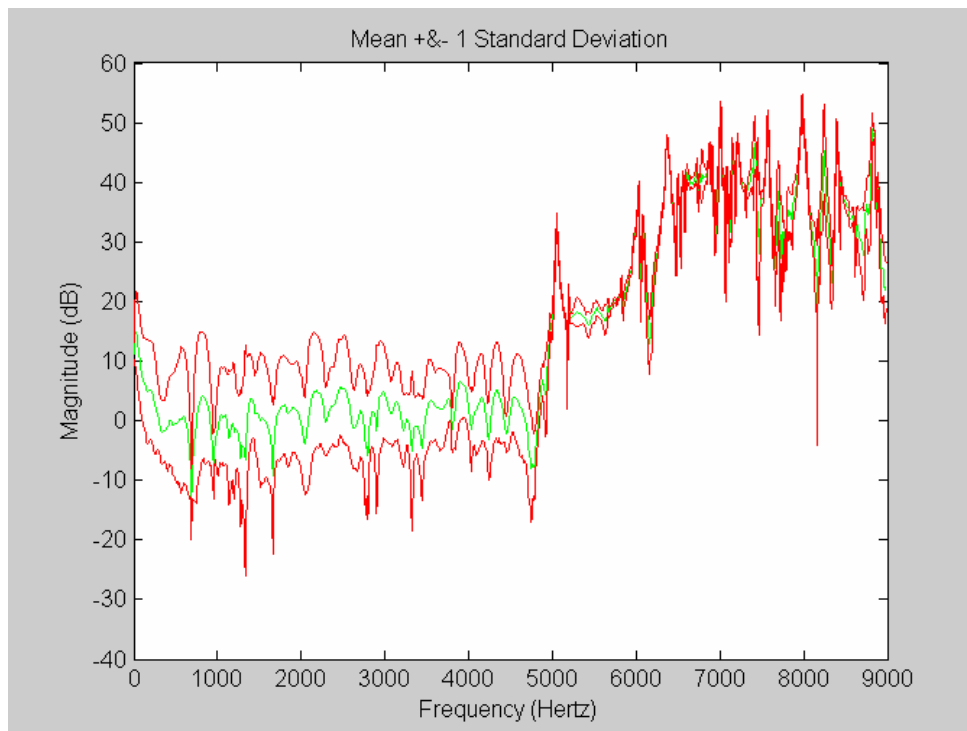
Figure 19: O2O tests, FRF21. (Mean and mean +/- one standard deviation.)
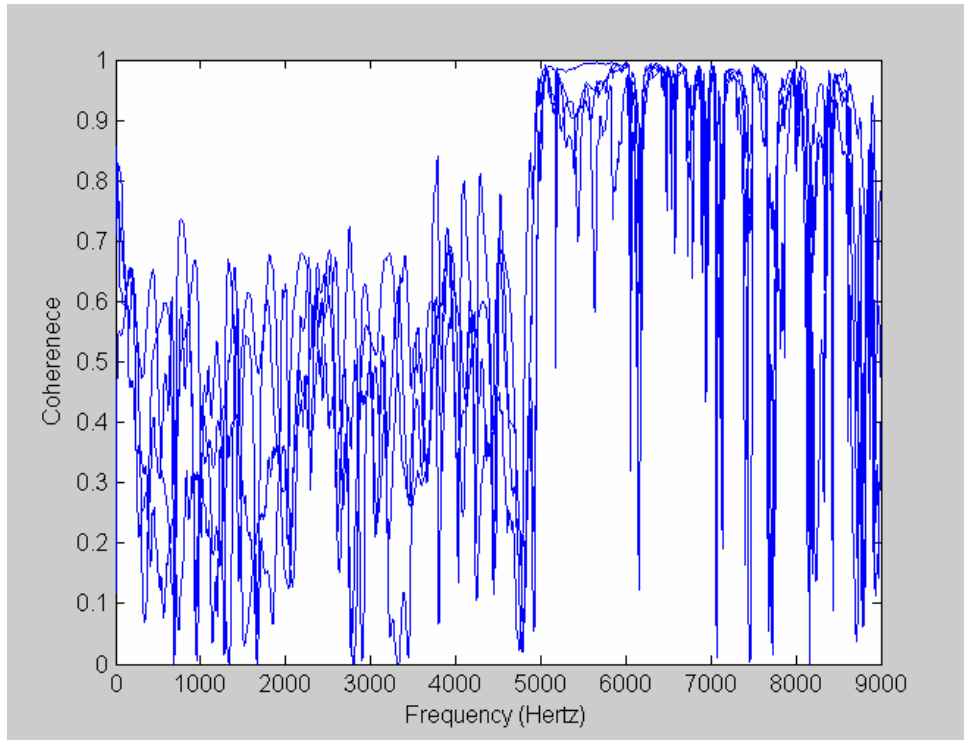
Figure 20: O2O coherence, FRF21. (All data sets collected.)
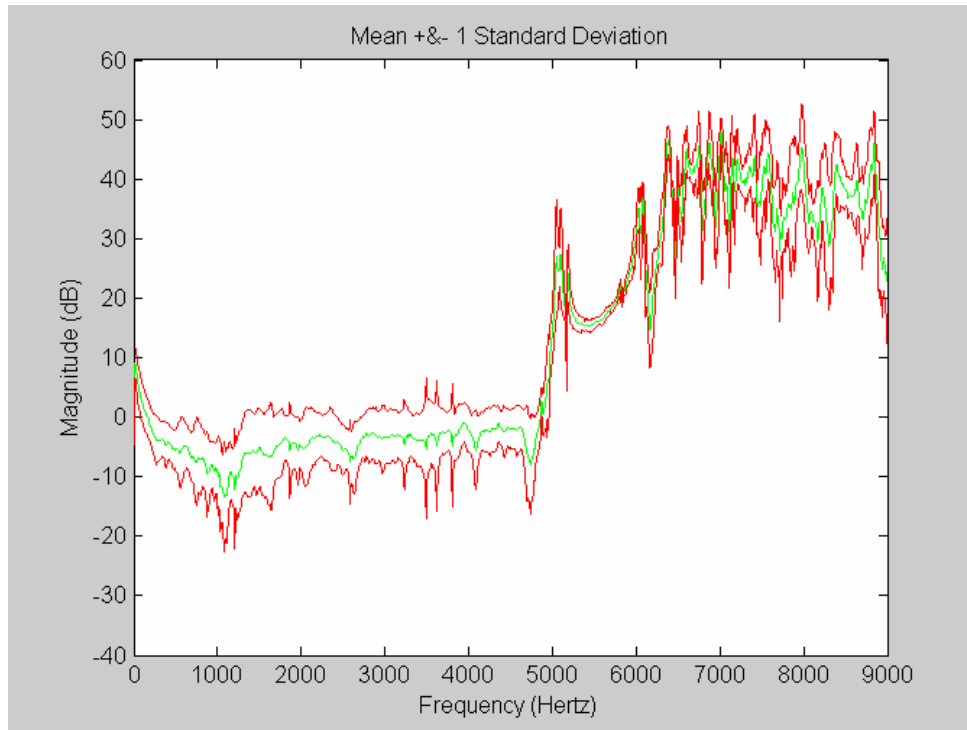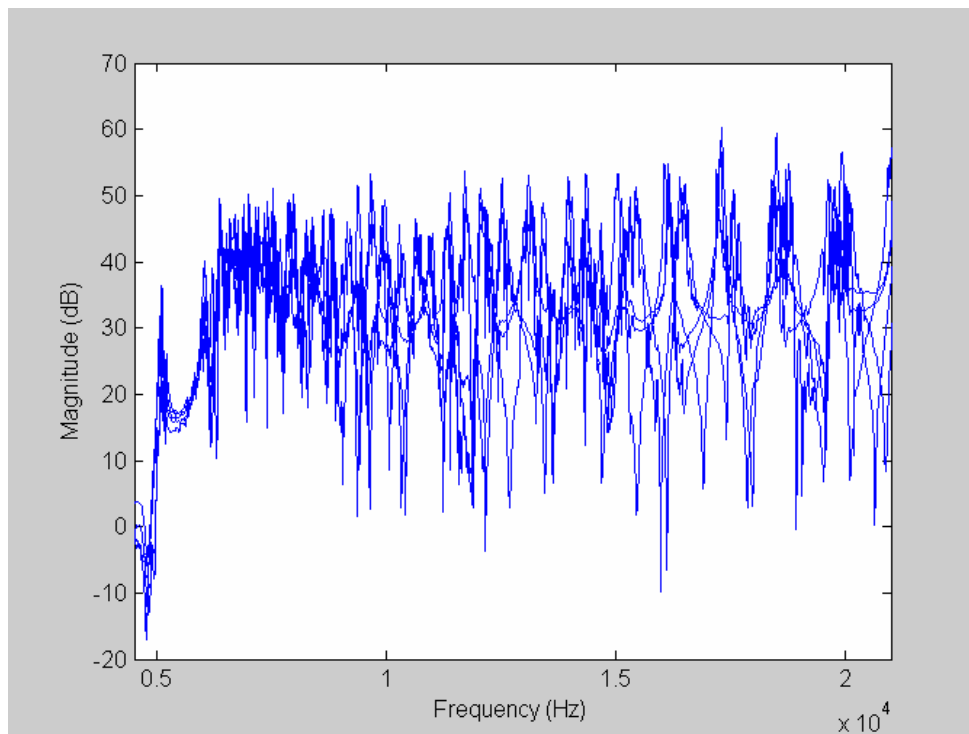

Figure 21: High-bandwidth tests, FRF21. (All data sets collected.)
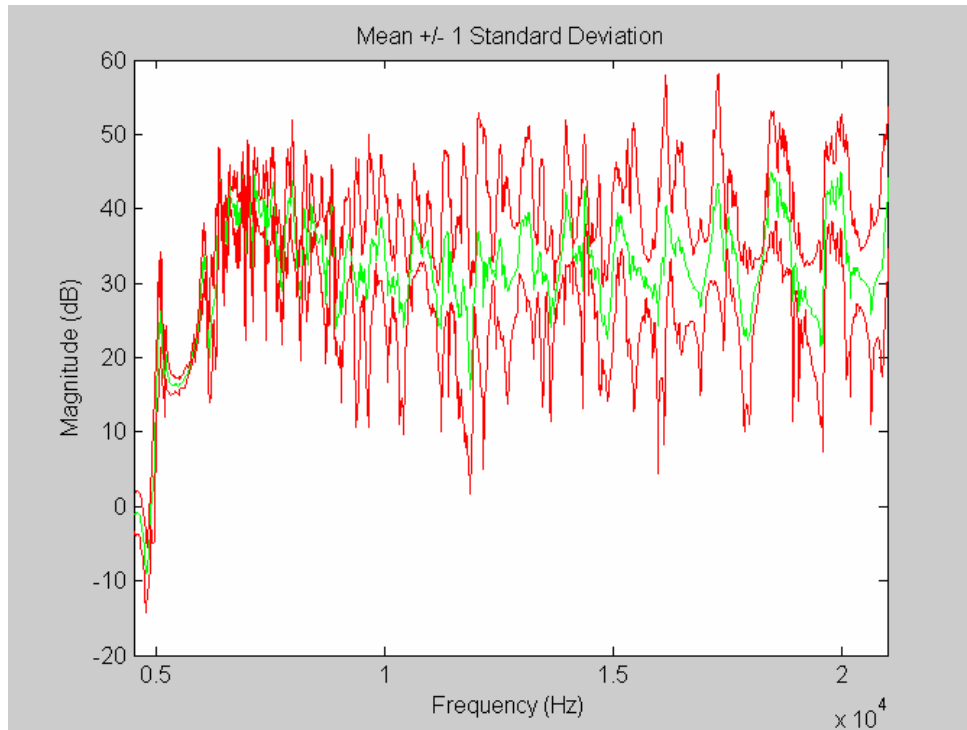
Figure 22: High-bandwidth tests, FRF21. (Mean and mean +/- one standard deviation.)
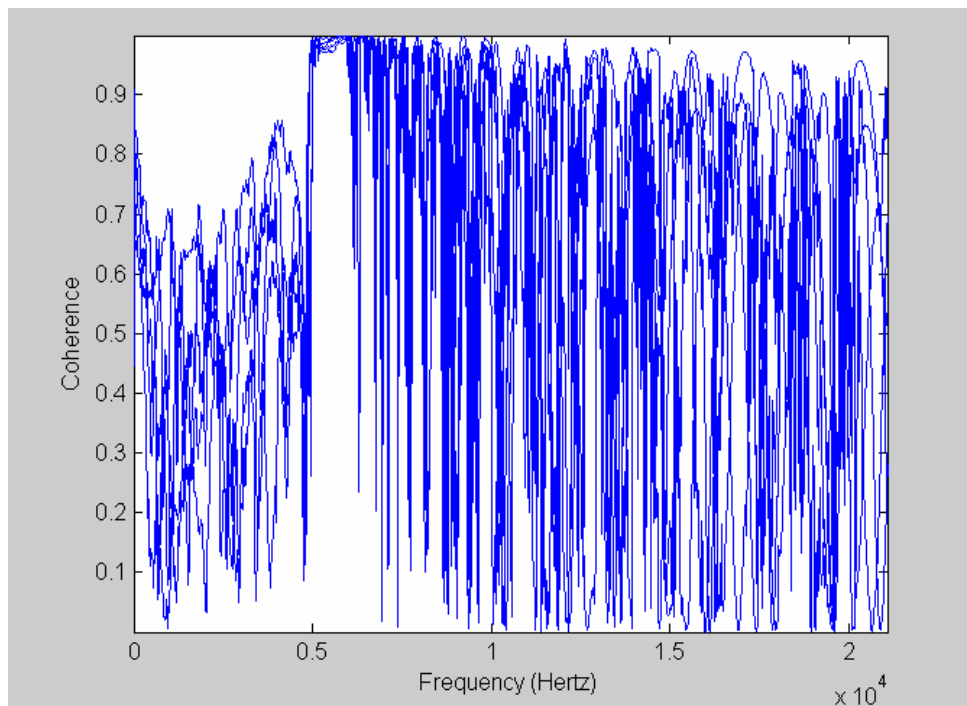
Figure 23: High-bandwidth coherence, FRF21. (All data sets collected.)

The figures above provide the first indication of how much variability is present in the data. To assess the level of variability in each of the test groups, a measurement of the deviation of each individual FRF from the mean FRF for the entire test group was found and is shown in Figure 24. The mean and standard deviation of these data within each group are then shown in Figure 25. Both indicators show that changing the test unit is, by far, the largest contributor to variability in the FRFs.
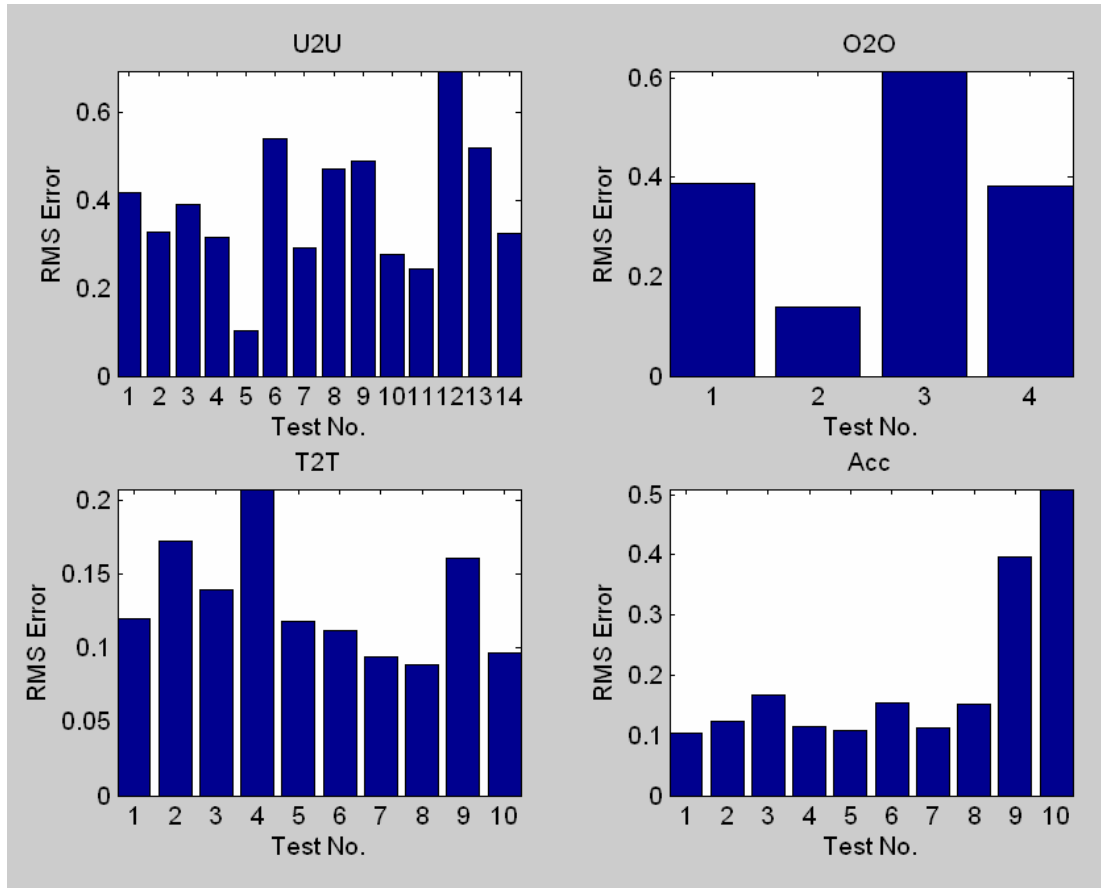
Figure 24: RMS deviation of each individual test from the mean of its test group.
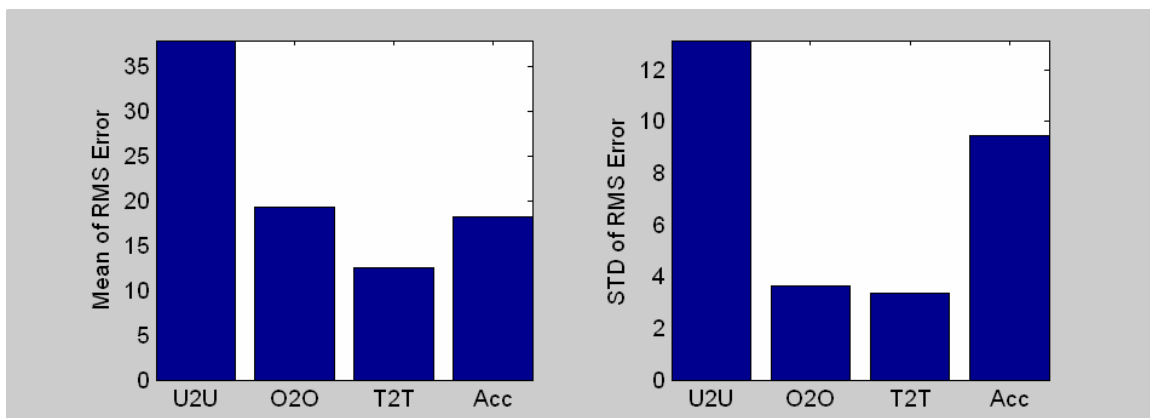
Figure 25: Mean and standard deviation of the RMS error within each group (based on Figure 24).

5.3   Feature Extraction for Variability Assessment

Now that we have collected the data and calculated the frequency response functions, we must form other methods for assessing the level of variation in the system response. We can make a direct comparison among the individual data sets by finding the correlation of either the time or frequency response data, as shown in Section 5.3.1. Another approach is to extract features from the data whose variation can be used to estimate the variation of the data. These features may also be more meaningful than the raw data, thus enhancing the interpretability of the data.

We examine three types of features here: Section 5.3.1 examines temporal and spectral moments, Section 5.3.2 uses principal component analysis, and Section 5.3.3 investigates ARMAX modeling.

5.3.1   Correlation

The correlation coefficient, *R(i,j)*, is a normalized measure of the strength of the linear relationship between two data sets, x_i and x_j:

$$R(i, j) = \frac{C(i, j)}{\sqrt{C(i,i)\, C(j, j)}}$$

(1)

where *C(i,j)* denotes the covariance between x_i and x_j:

$$C(i, j) = E\left[(x_i - \mu_i)(x_j - \mu_j)\right]$$

(2)

and *E* is the mathematical expectation, with $\mu_i = E(x_i)$. Uncorrelated data sets result in a correlation coefficient of zero, whereas perfectly correlated data sets have a coefficient of one.

Within each test group, a matrix of correlation coefficients is computed, describing the relationship between each data set and each of the remaining data sets. We then average these values to obtain a mean estimate of the correlation between data sets in a given test group. Figure 26 shows the mean correlation coefficient for each of the following data: the acceleration measurements for Channels 2, 3, and 4, and the impulse response measurements for Channels 2, 3, and 4 (see Appendix C for the definition of the impulse response). The results show that the lowest level of correlation (or highest level of variation) occurs between data sets in which the unit is changed (U2U), whereas the best correlation is found between data sets in which only the operator (O2O) or the test setup (T2T) is changed. Also note that the correlation coefficients for the impulse response are higher than those for the acceleration response. One would expect this result, because the impulse response data eliminates variations in the data caused by differences in the system excitation.

These calculations are then repeated for the spectral data, which consists of the auto-spectral density functions for each channel (G22, G33, and G44), and the FRFs (FRF21, FRF31, and FRF41). Refer to Appendix C for the definition of these functions. The results from these calculations are very similar to those obtained for the time histories.
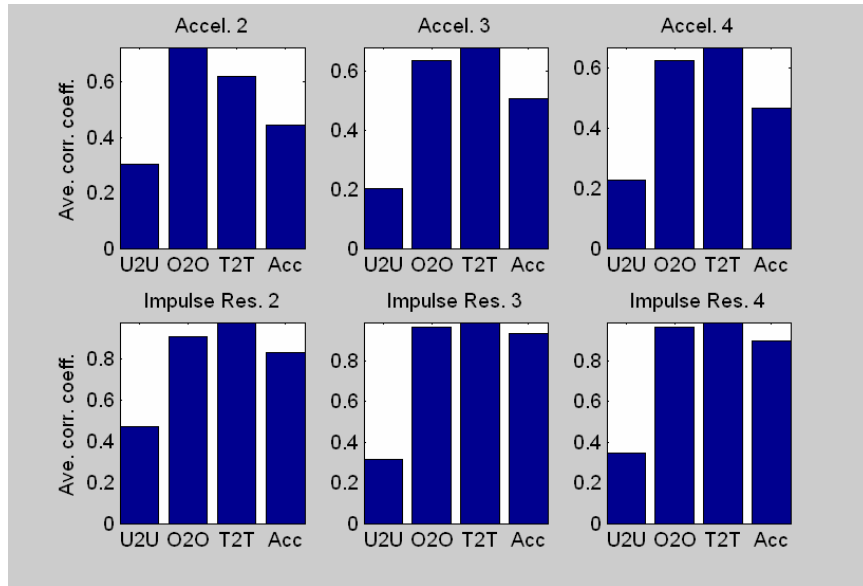
Figure 26: Mean correlation of time-response data.
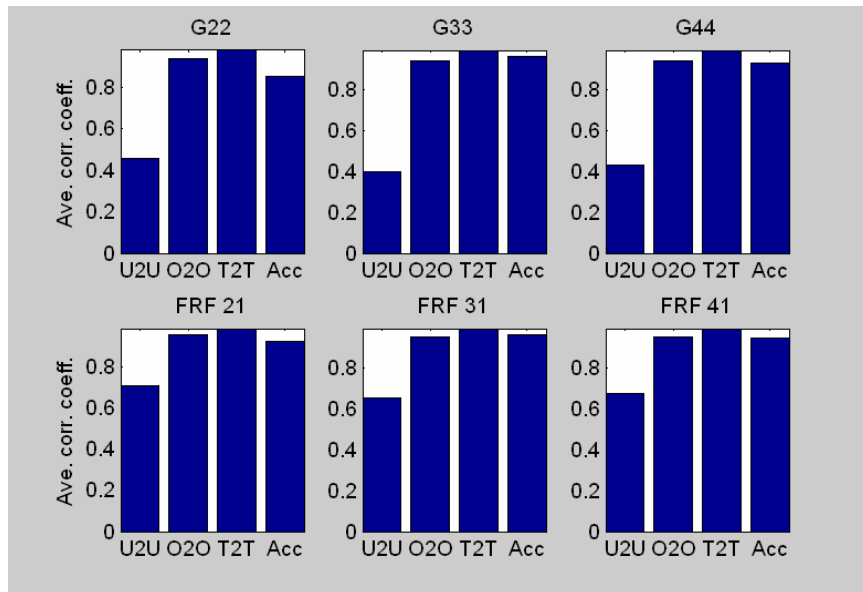
Figure 27: Mean correlation of frequency-domain data.

5.3.2 Temporal and Spectral Moments

Temporal moments are a measure of the time statistics of a signal. They are used here to find another means for estimating the variability in the data. We focused on only the first three temporal moments, which are [5]:

- E = Energy, $[g^2]$.

- *Tau* or T = Delay to the centroid of data, [sec].

- D = Central normalized RMS duration, [sec].

The features *E*, *Tau*, and *D* are calculated as follows:

$$E = \sum_{0 \le t \le N} (x(t))^2 \qquad (3)$$

$$T = \frac{1}{E} \sum_{0 \le t \le N} t \cdot (x(t))^2 \qquad (4)$$

$$D^2 = \frac{1}{E} \sum_{0 \le t \le N} t^2 \cdot (x(t))^2 - T^2 \qquad (5)$$

where *x(t)* is the impulse-response-time history for this analysis. We extracted the three temporal moments for each impulse-response measurement on Channel 2. Then, we assessed the standard deviation of these indicators inside each test group. As shown in Figure 28, the relative levels of variation between test groups are the same for each of the three temporal moments. U2U variation far outweighs the effects of a different operator (O2O), test setup (T2T), or Acc. However, one would expect the variation in the test data resulting from Acc to be higher than that for T2T, since the float needs to be removed from the rope ring to change the location of the accelerometers. There appears to be a slight increase in variation of the temporal moments for the Acc case over the T2T, but the increase is not significant. This seems to indicate that the Acc has no significant effect on the response measurement for the system.
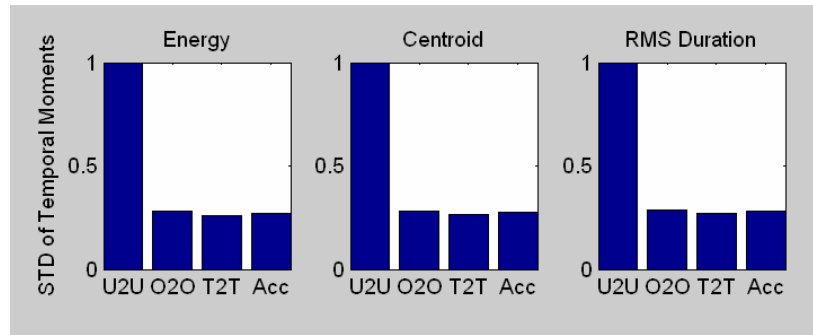
Figure 28: Normalized standard deviation of *E, Tau*, and *D* for impulse responses from Channel 2.

By substituting frequency for time in equations 3–5, we find the spectral moments of the response data. The interpretation is the same, with energy being the energy in the frequency domain, and similarly for the centroid and RMS duration. Figure 29 gives the normalized standard deviation of the spectral moments for the frequency-response function from Channel 2 for each test group. The results are similar to the temporal moments, though with a slight increase in the variation caused by Acc.
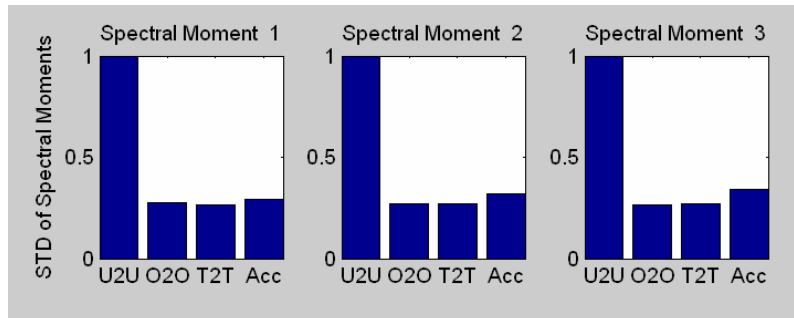
Figure 29: Normalized standard deviation of spectral moments for FRF21.

From this analysis we conclude that the most significant effect on the data comes from changing the unit that is tested. The three remaining sources of variability (operator, test repeatability, Acc) appear to contribute equally to the variability in both the time and frequency domains.

5.3.3   Principal Component Analysis

The next feature we examined was the principal components of the impulse and frequency-response functions from Channel 2. Given N samples of data in p dimensions, $(x_1, x_2, \ldots, x_p)$, the principal component analysis (PCA) seeks to project the data into a new p-dimensional set of Cartesian coordinates $(z_1, z_2, \ldots, z_p)$ by a linear transformation [6]. The goal of PCA is to conduct data reduction in such a way that this linear combination of the original variables contains as much of the total variance as possible when projected into the reduced space.

The principle coordinates are calculated as follows: Given data $x_i = [x_{1i}, x_{2i}, \ldots, x_{pi}]^T$, where the index I varies from one to N, the covariance matrix Σ is formed:

$$\Sigma = \sum_{i=1}^{N} (\mathbf{x}_i - \overline{\mathbf{x}})(\mathbf{x}_i - \overline{\mathbf{x}})^T \tag{6}$$

where $\overline{\mathbf{x}}$ denotes the mean vector of the x_i's. Because it is, by definition, symmetric and positive semidefinite, the covariance matrix can then be decomposed into a set of eigenvalues and eigenvectors:

$$\Sigma = \mathbf{V}\Lambda\mathbf{V}^T \tag{7}$$

where Λ is a diagonal matrix containing the ranked eigenvalues of Σ, and $\mathbf{V}$ is the matrix containing the corresponding eigenvectors. Note that the singular value decomposition can be used for this step. The transformation to principal components is then:

$$\mathbf{z}_i = \mathbf{V}^T(\mathbf{x}_i - \overline{\mathbf{x}}) \tag{8}$$

This means that the coordinates z_i are the projection of the original x_i onto the eigenvectors defined by the columns of matrix *V*. These eigenvectors are called the principal components, and the coordinates z_i are called the *scores*.

There are as many principal components as there are data points, but the first principal component accounts for as much of the variability in the data as possible. Each succeeding component accounts for as much of the remaining variability as possible, and so on. Therefore, only a few principal components are needed to represent the data. The coefficients in the eigenvector matrix that relate the original functions to the principal components are the features of interest here. In other words, the variation of these coefficients is used to assess the variability of the data sets within a test group.

The first nine principal components of the impulse response at Channel 2 are shown in Figure 30 and their cumulative variance in Table 3.
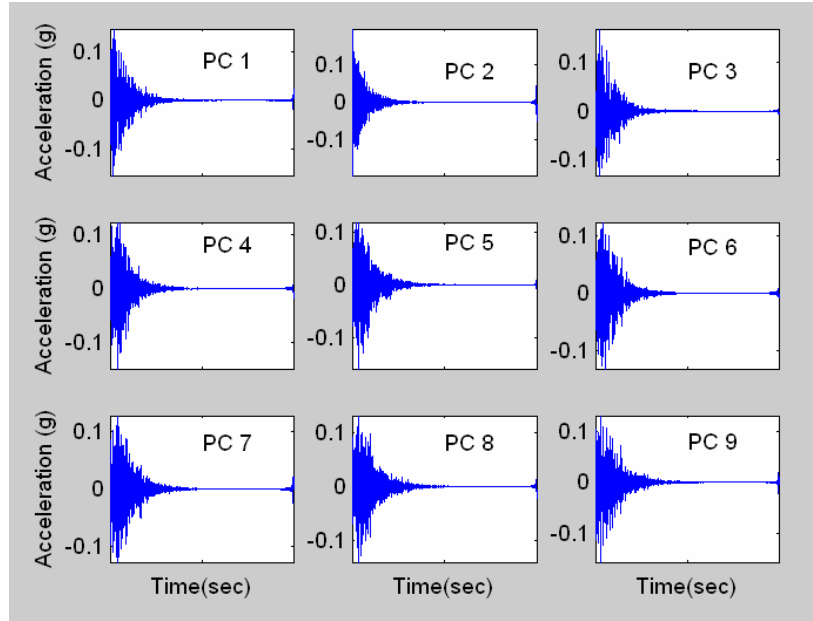
Figure 30: First nine principal components for the impulse responses at Channel 2.

Table 3: Cumulative variance of the principal components for impulse responses.

Principal Component	Cumulative Variance
1	28.25%
2	45.37%
3	57.81%
4	64.20%
5	70.19%
6	75.42%
7	79.87%
8	83.54%
9	86.65%

As shown in Table 3, the first nine principal components account for almost 87% of the variability in the data. Visually, there is little significance in the principal components themselves. The principal component coefficients are used to assess the variability in the data within each test group by examining the standard deviation of these coefficients.

Figure 31 shows that the relative variations between the test groups are similar for all but the second principal component, with U2U variability again being the highest.
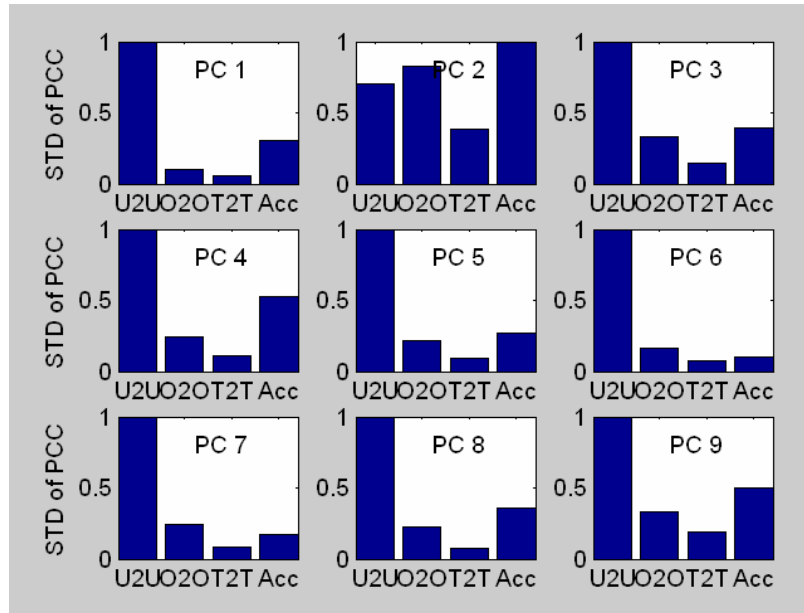
Figure 31: Normalized standard deviation of PCA coefficients for impulse responses at Channel 2.

Upon examination of the Fourier transform of the first two principal components, shown in Figure 32, the reason for the deviation of principal component 2 is understood. The second principal component has its highest magnitude in the upper frequencies of the frequency spectrum. Therefore, it is looking for variations in the upper frequency levels foremost, which will most likely be dominated by noise rather than modes. The variation of the coefficients pertaining to the second principal component are significant, because all tests have noise present and do not follow the general patterns of the other principal components.
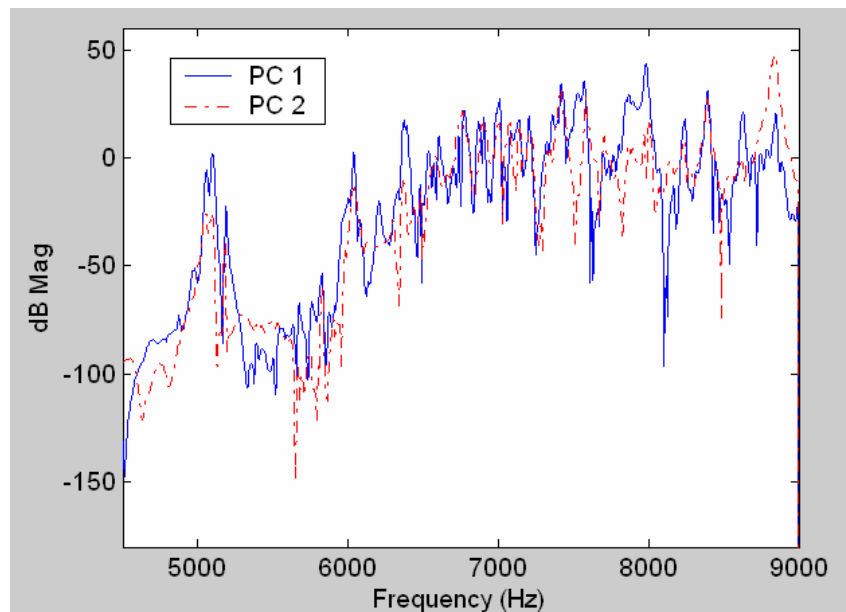
Figure 32: Fourier transform of principal components 1 and 2.

We repeated the principal component analysis for the frequency response functions from Channel 2. The first component appears to encompass more of the variability in the data (Table 4) than the first component of the impulse-response data (Table 3). The resulting principal component vectors are shown in Figure 33, and the variation between the coefficients within a test group in Figure 34. Note that only the magnitude of the FRF is used to extract the principal components.

Table 4: Cumulative variance of the principal components for FRF21.

Principal Component	Cumulative Variance
1	35.92%
2	48.59%
3	58.01%
4	65.30%
5	69.62%
6	73.44%
7	76.21%
8	78.49%
9	80.63%
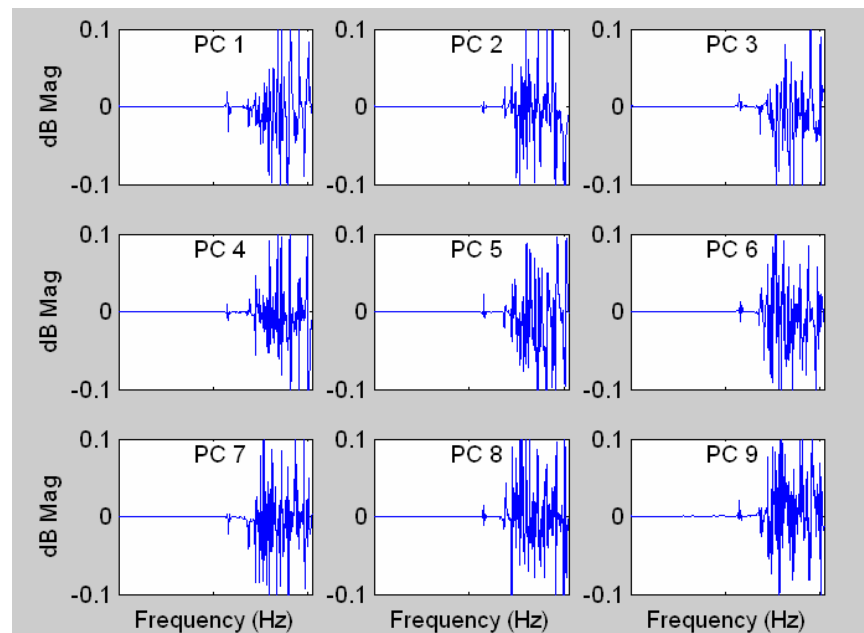
Figure 33: First nine principal components for FRF21.
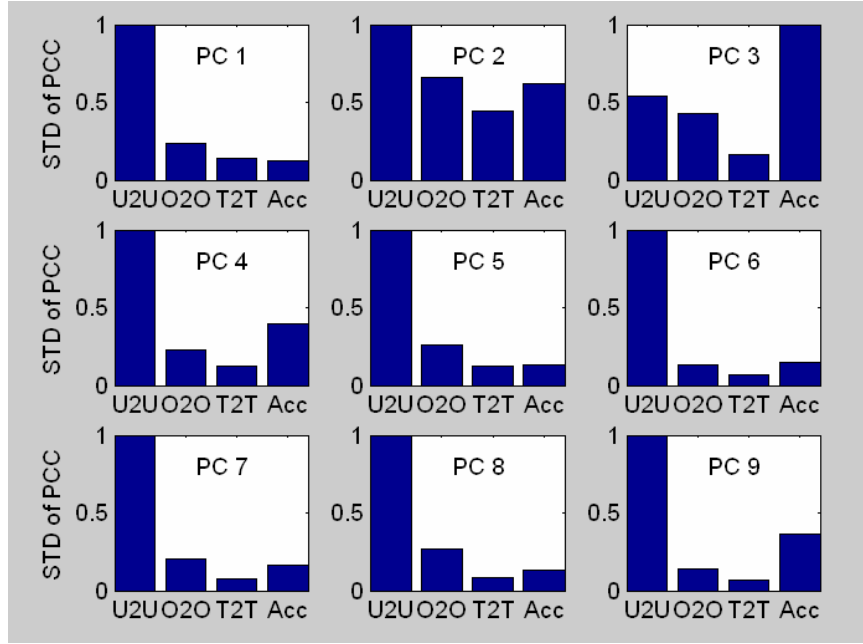
Figure 34: Variability of PCA coefficients for FRF21.

From this analysis, we can draw conclusions similar to the previous sections. In the majority of the principal components, changing the unit affects the response of the system more than any other factor. Acc in general comes in second, then changing the operator, and finally test repetition. Not all of the principal components show the same result, but the majority shows this pattern.

5.3.4 ARMAX Modeling

An autoregressive moving-average model with exogenous inputs, or ARMAX model, is a parametric representation of time series. It approximates a response *y(t)* using a linear difference equation [7]:

$$
\begin{aligned}
y(t) + a_1 y(t-1) + \mathrm{K} + a_{na} y(t-na) &= b_1 u(t-nk) + \mathrm{K} + \\
b_{nb} u(t-nk-nb+1) + c_1 e(t-1) &+ \mathrm{K} + c_{nc} e(t-nc)
\end{aligned}
\tag{6}
$$

which relates the current output *y(t)* to a finite number of past outputs *y(t-k)*, inputs *u(t-k)*, and white noise *e(t-k)*. For this analysis, we formed a model relating the acceleration response of the float from Channel 2, *y(t)*, to past time points in the acceleration, as well as the impulse excitation, *u(t)*. We used the same model form for each of the data sets, which consists of thirteen a_k coefficients, seven b_k coefficients, one c_k coefficient, and a zero time delay (*nk* = 0). We chose the coefficient order based on the general guideline that the size, and the resulting fitting error, not be too large,.

Once formed, the ARMAX model can be simulated to produce the approximated output. We hypothesized that the error between the ARMAX estimation of model output and the actual value, which in this case is the acceleration response from Channel 2, can be used to examine variability for each group of tests performed. This variation is shown in Figure 35, using the standard deviation of the error vector. We can also asses variability within the test groups from the coefficients of the model (a_k and b_k). Because there are so many coefficients to compare, an easy way to examine them is to find their principal components. Figure 36 shows the standard deviation of the principal components found for both the a_k and b_k coefficients inside each of the four test groups.
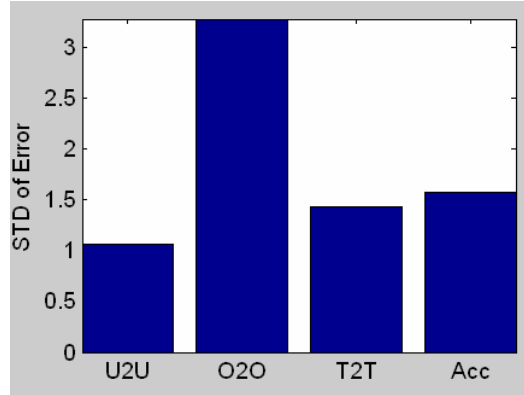
Figure 35: Variability of the fitting error obtained from ARMAX models.
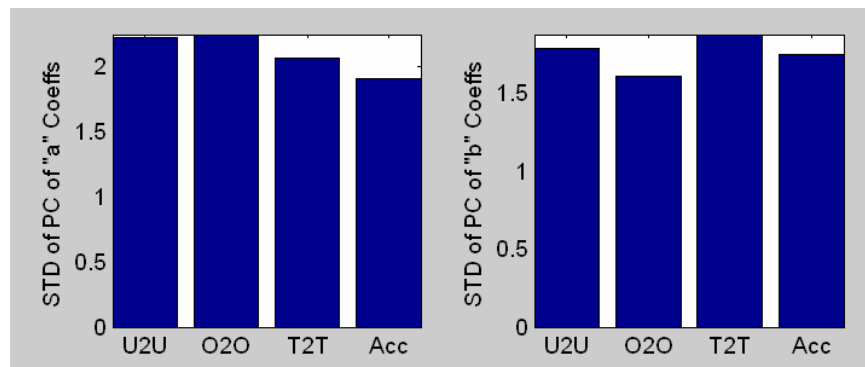
Figure 36: Variability of the principal component analysis of ARMAX model coefficients.

Unfortunately, both of these variability assessments seem to contradict the results in all of the previous sections. Further investigation revealed that changing the model order creates a different relative relationship between the standard deviations among the groups. These results indicate that ARMAX modeling is not appropriate for determining variability in the modal response data, because variability and model-fitting issues are confounded.

5.4   ERA Fit

ERA is an eigensystem realization algorithm [8] that converts time-domain data to modal frequencies, modal damping ratios, and mode shapes. We used the ERA fit to determine the spread of modal frequencies obtained for all tests. We restricted our analysis to the first four modes of the system; Figure 37 shows the results, with frequency on the horizontal axis, damping on the vertical axis, and various symbols representing the results from all data sets collected. A close-up of the data for each mode can be seen in Figure 38 through Figure 41.

Figure 42 displays the standard deviation for each of the four modes shown in the above plots. As expected, the standard deviations of the U2U and Acc tests are in general higher than the standard deviations of the other tests. However, Acc variability is higher than U2U variability for two of the modes, which contradicts the assumption that U2U variability should encompass Acc variability. Also, T2T variability is larger than Acc for the first mode, which also contradicts the assumption that Acc variability should encompass T2T variability.
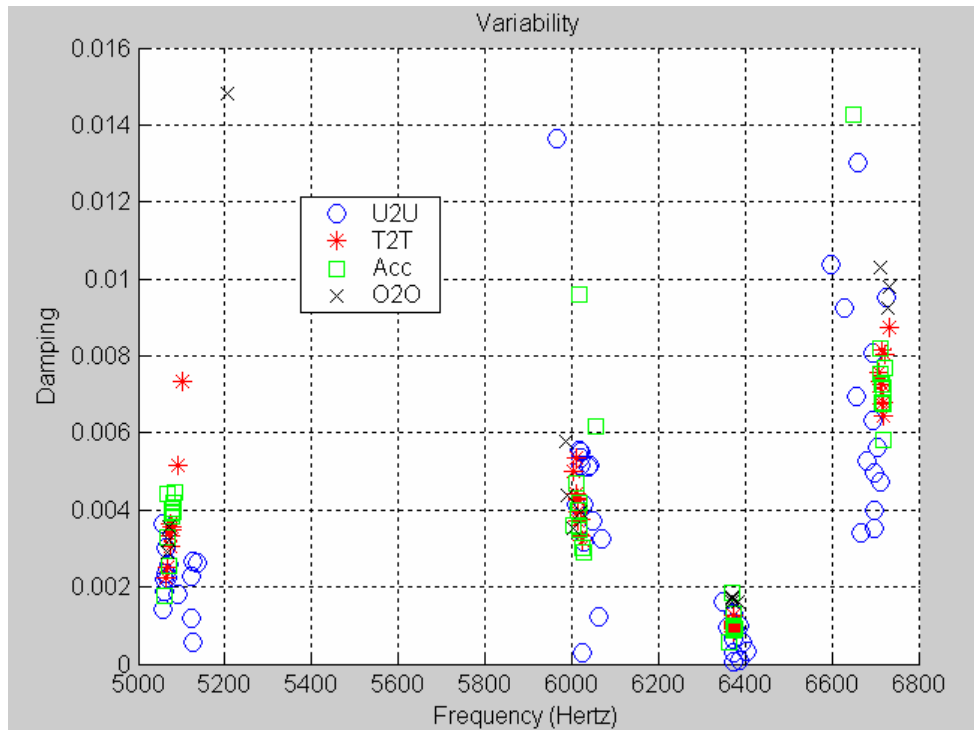
Figure 37: ERA-fit results showing frequency and damping variability for the first four modes.
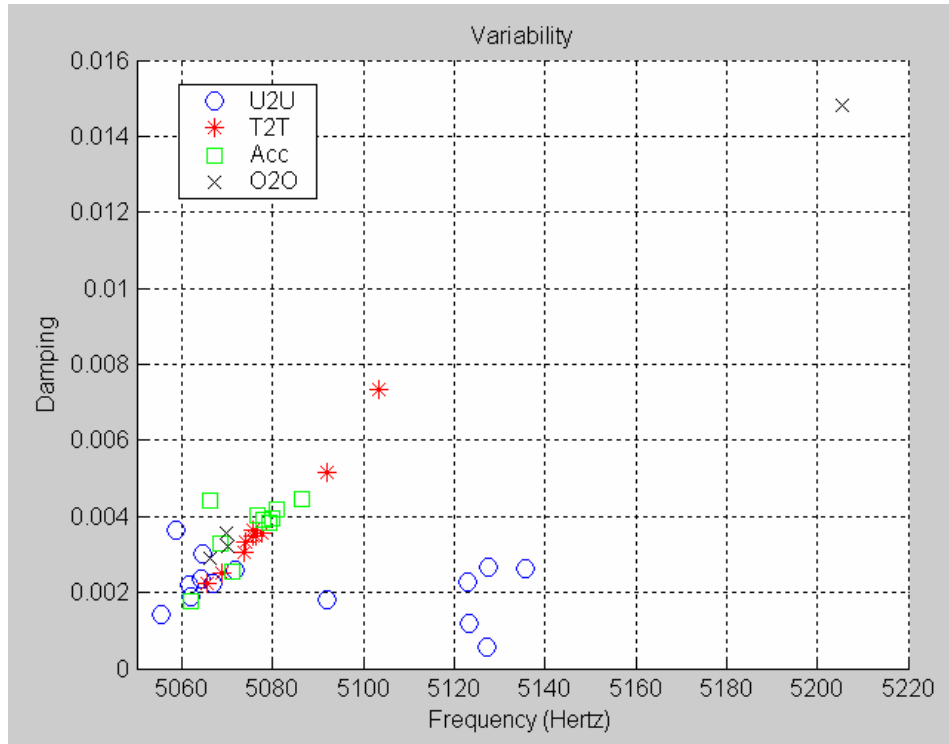
Figure 38: ERA-fit results; frequency and damping variability for the first mode.
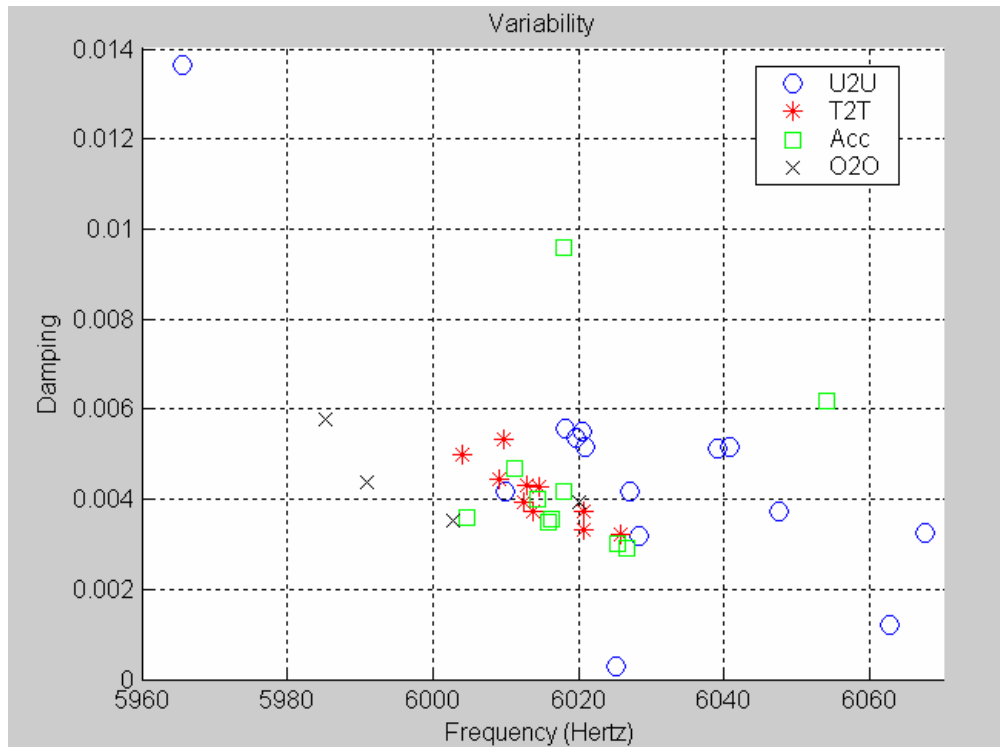
Figure 39: ERA-fit results; frequency and damping variability for the second mode.
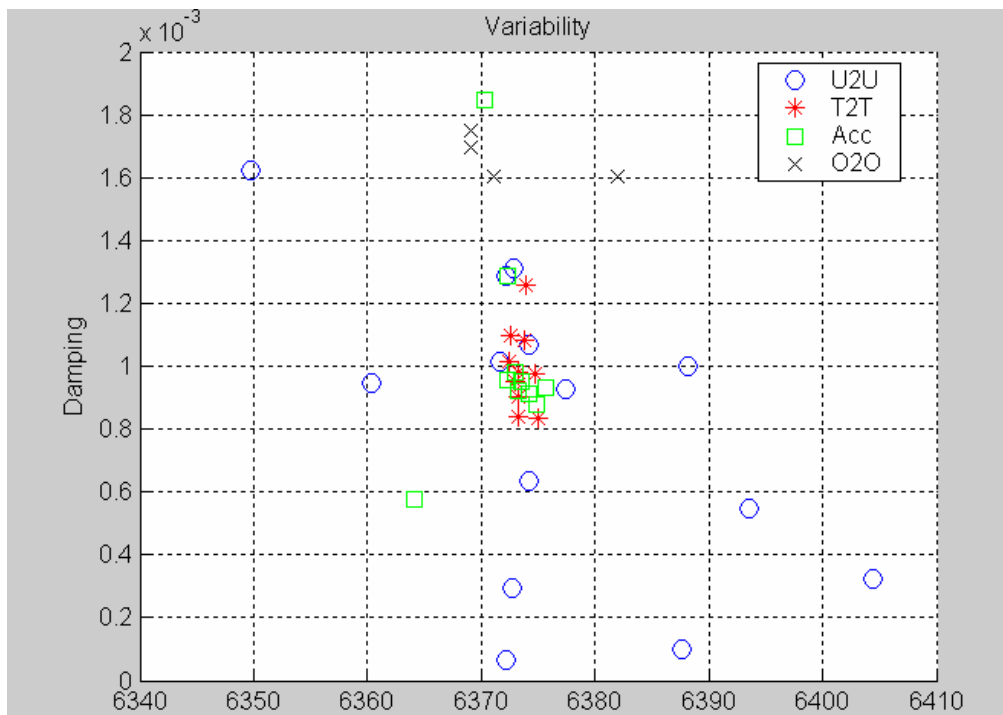
Figure 40: ERA-fit results; frequency and damping variability for the third mode.
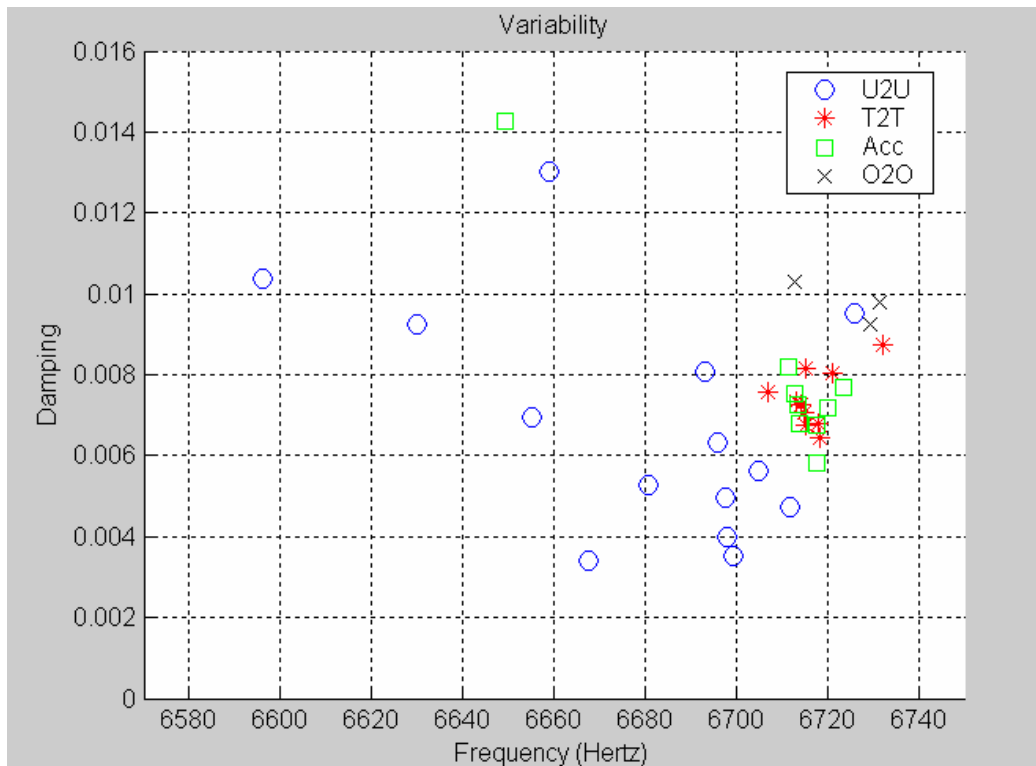
Figure 41: ERA-fit results; frequency and damping variability for the fourth mode.
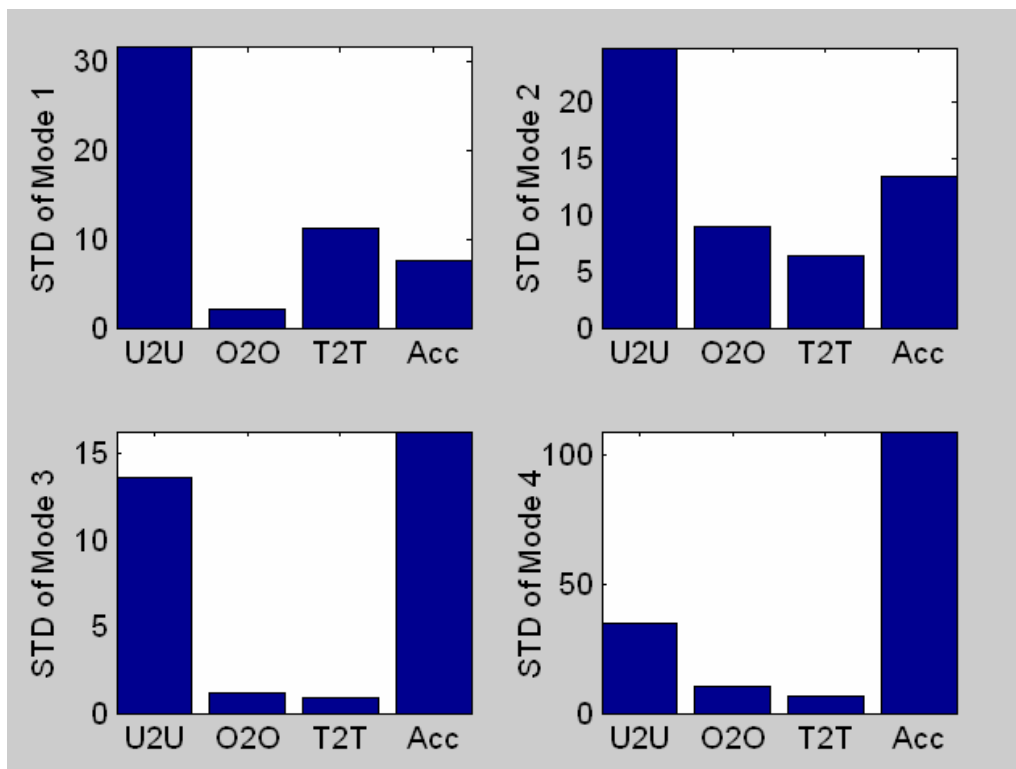
Figure 42: ERA-fit results: frequency variability of the first four modes.

We also used the ERA to automatically identify a specified number of modes in the high-bandwidth data set. Shown in Table 5, the modes identified for each test are matched, starting at the 5,000-Hz mode and stopping after 20 identified modes. All resonant frequencies listed in Table 5 are listed in units of hertz, while the standard deviation values are listed in percents of the mean values (last column). The algorithm finds the most pronounced resonant peaks up to the model order specified, and a stabilization plot is generated that shows the model order—or number of modes to be identified—on the y axis and frequency on the x axis. After studying which modes are consistently identified when an increasingly higher model order is requested, we eliminated the falsely identified readings. We also included for comparison in the second column of Table 5 the resonant peaks identified from the FRF plot for Test 1 (using float number 16). Each test examines a different float, so the variability in the frequency measurements should be similar to the U2U variability observed previously. The ability to consistently find these higher modes shows that we can also use this region of the frequency response of the system to assess which factors contribute most to the variability in the data. We believe that not enough tests have been performed at this point, however, to perform such an analysis with statistical significance.

Table 5: List of modal frequencies (hertz).

Mode Number	Test 1 (FRF Plot)	Test 1 (ERA)	Test 2 (ERA)	Test 3 (ERA)	Test 4 (ERA)	Test 5 (ERA)	Average	Standard Deviation (%)
1	5,050.0	5,004.7	5,095.3	5,017.2	5,027.7	5,126.5	5,053.6	0.947
2	6,030.0	6,318.1	6,399.5	6,323.3	6,150.8	6,105.3	6,221.2	2.347
3	6,370.0	6,373.8	6,694.9	6,398.6	6,625.9	6,583.7	6,507.8	2.212
4	7,012.0	7,119.6	7,379.7	7,198.8	7,249.1	7,256.5	7,202.6	1.752
5	7,980.0	7,920.8	8,187.1	7,960.7	7,962.9	7,882.9	7,982.4	1.331
6	8,835.0	8,778.3	8,795.2	8,803.7	8,660.3	8,930.7	8,800.5	0.995
7	9,970.0	9,773.5	9,079.7	9,953.1	9,478.2	8,980.2	9,539.1	4.543
8	10,635.0	10,168.0	9,650.0	10,314.0	10,301.0	9,659.2	10,121.2	3.880
9	11,355.0	11,229.0	10,887.0	11,122.0	11,188.0	10,933.0	11,119.0	1.614
10	12,052.0	12,151.0	11,690.0	12,094.0	11,344.0	11,767.0	11,849.7	2.613
11	13,100.0	13,100.0	12,491.0	13,109.0	12,148.0	12,555.0	12,750.5	3.217
12	13,302.0	13,397.0	13,452.0	13,975.0	13,108.0	13,742.0	13,496.0	2.319
13	13,965.0	13,973.0	14,386.0	14,393.0	14,239.0	14,404.0	14,226.7	1.466
14	15,117.0	15,025.0	15,390.0	15,078.0	15,030.0	15,427.0	15,177.8	1.200
15	16,160.0	16,173.0	16,427.0	16,160.0	16,098.0	16,406.0	16,237.3	0.871
16	17,310.0	17,303.0	17,560.0	17,285.0	17,225.0	17,529.0	17,368.7	0.805
17	18,505.0	18,500.0	17,933.0	18,495.0	18,193.0	17,555.0	18,196.8	2.139
18	18,655.0	18,935.0	18,674.0	18,753.0	18,411.0	18,805.0	18,705.5	0.942
19	19,770.0	19,712.0	19,198.0	19,884.0	19,223.0	19,475.0	19,543.7	1.487
20	19,992.0	19,972.0	19,902.0	19,945.0	19,663.0	19,904.0	19,896.3	0.602

5.5   Mass Correlation

We found the nominally identical floats to have slightly different masses. In addition, the measurements show that the masses of the floats have two distinct groupings. We therefore needed to determine if the mass affects the identified frequencies. The sample of floats examined includes five floats from the lower mass group and nine floats from the higher mass group. The mass correlation is illustrated in Figure 43. This plot of float mass versus identified frequency reveals that the frequency values for the lower-mass floats are more variable than those for the higher-mass floats. For the first mode, the amount of variability in the frequency measurements is smaller, and we observed a clear relationship between float mass and modal frequency. The relationship is negative, as it should be, because an increase in mass decreases the modal frequency value.
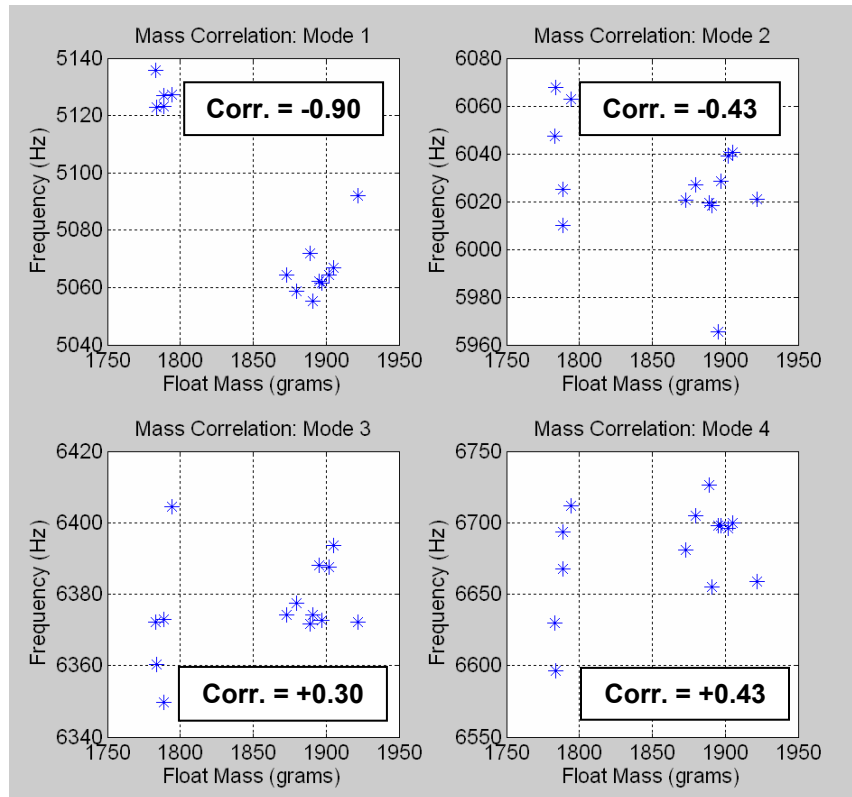
Figure 43: Mass correlation for the first four modes.

Figure 44 looks at how much the mass affects the variability of the modal frequencies between floats. This figure shows that for modes 2–4, the higher-mass floats have more variation in their modal frequencies. However, the higher-mass floats also have more variation in their mass values, which should cause more variation in the frequency values if mass and frequency were correlated. Only the first mode shows a strong correlation to the mass of the float, and this is the one mode that has more variability in the smaller-mass floats.
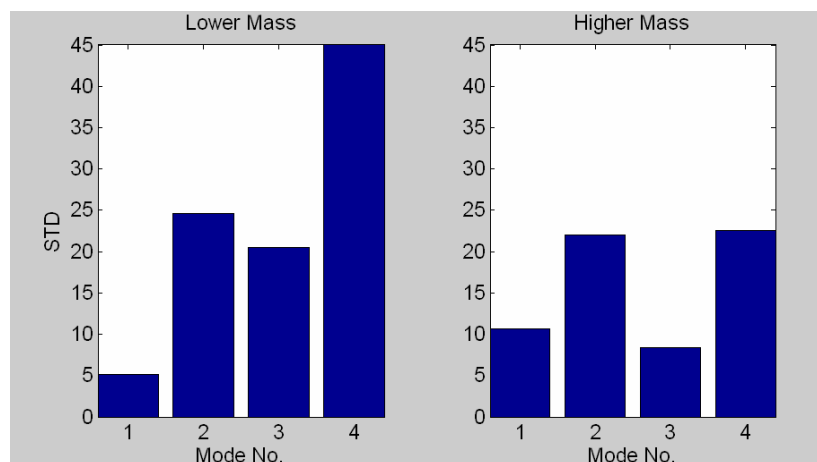
Figure 44: Standard deviation of modal frequencies segregated by low- and high-mass floats.

6. Analytical Resonant Frequencies of a Thin Spherical Shell

6.1 Background

Scientists have reported numerous theoretical investigations of the natural frequencies for complete spherical shells over the past four decades. However, few have attempted to correlate the theoretical results, both for axisymmetric and nonaxisymmetric modes of response. This report details a series of modal tests performed on commercially available, stainless steel marine floats. The floats are complete spherical shells, but they contain imperfections [2].

In this section, we compare the natural frequencies obtained with axisymmetric and nonaxisymmetric theories of vibration of perfectly spherical shells. Because of the imperfections, we anticipate the phenomenon known as the "splitting" of frequencies of nonaxisymmetric. We verified the correlation of natural frequencies with earlier theoretical results for the first few modes, and the presence of the frequency-splitting phenomenon is suggested. The need for additional related work is indicated.

6.2 Analytical Frequency Results for a Perfect Spherical Shell

The modal frequencies for a thin spherical shell are given by:

$$f_i = \frac{\lambda_i}{2\pi R}\left[\frac{E}{\mu(1-\upsilon^2)}\right]^{1/2} \tag{7}$$

where f_i is the frequency in hertz, R is the midsurface radius, μ is the density, E is the modulus of elasticity, υ is the Poisson's ratio, and h is the shell thickness. Appendix D lists the material and geometric parameters for the floats studied in this report. The parameter λ_i in equation (7) takes on a variety of forms depending upon the shell theory used. For purely membrane response (Baker [9]):

$$\lambda_i = \left[\frac{2(1+\upsilon)}{1+h^2/(12R^2)}\right]^{1/2} \tag{8}$$

$$\lambda_i = \left[\frac{(1-\upsilon)(i^2+i-2)}{2+5h^2/(6R^2)}\right]^{1/2} \quad \text{for } i = 1, 2, 3, \ldots \tag{9}$$

$$\lambda_i = \frac{1}{\sqrt{2}}\left[(i^2+i+1+3\upsilon)\pm\left[(i^2+i+1+3\upsilon)^2 - 4(1-\upsilon^2)(i^2+i-2)\right]^{1/2}\right]^{1/2} \quad \text{for } i = 0, 1, 2, \ldots \tag{10}$$

Equation (8) gives the fundamental radial mode, equation (9) is for torsional modes, and equation (10) gives the radial-tangential modes. This theory ignores bending. For a higher-order shell theory including the effects of bending, refer to Wilkinson [10].

A comparison of the frequencies extracted using the various approaches is beyond the scope of the current analysis. For now, we examine how one set of analytical frequencies (including the effects of bending) compares to the experimentally extracted values.

6.3 A Comparison of Observed Vibration Frequencies With Predictions

As described in Section 5.4, an ERA fit is performed on the FRF data to determine the natural frequencies of the first four modes, and the results for these four modes are summarized in Table 5 through Table 8, respectively. The four tables show that U2U variation and Acc are the greatest sources of frequency variability.

We also compare the results from the ERA fit to the corresponding analytical results in Tables 5–8. Note that we compare the identified frequencies to those of a perfect spherical shell. The frequencies lie on the lower (primarily, bending) branch and correspond to indices i = 2, 3, 4, and 6, respectively. (The first mode, i =1, is the rigid-body mode of zero frequency. The mode corresponding to i = 5 is not extracted.) We observed that, in all cases, differences between analytical and experimental results are less than one percent. In fact, the test-analysis differences are considerably less than one percent in most cases. We attribute these differences to variations in geometry and mass. In addition, we anticipated variation because of the splitting of frequencies, although the magnitude of splitting is unknown at this point. We could evaluate the magnitude of splitting by detailed finite element calculations that include a representation of the variation in radius and thickness of the spheres.

Table 6: First mode comparisons of measured and predicted frequencies.

	Test (Mean)	Analytical (i = 2, lower branch)	Frequency Difference (%)
U2U	5,088.09	5,078.00	0.20
T2T	5,078.22	5,078.00	0.00
Acc	5,074.86	5,078.00	0.06
O2O	5,068.65	5,078.00	0.18

Table 7: Second mode comparisons of measured and predicted frequencies.

	Test (Mean)	Analytical (i = 3, lower branch)	Frequency Difference (%)
U2U	6,028.06	6,005.00	0.38
T2T	6,014.38	6,005.00	0.16
Acc	6,020.45	6,005.00	0.26
O2O	5,992.98	6,005.00	0.20

Table 8: Third mode comparisons of measured and predicted frequencies.

	Test (Mean)	Analytical (i = 4, lower branch)	Frequency Difference (%)
U2U	6,378.63	6,378.00	0.02
T2T	6,373.50	6,378.00	0.07
Acc	6,367.53	6,378.00	0.16
O2O	6,369.80	6,378.00	0.13

Table 9: Fourth mode comparisons of measured and predicted frequencies.

	Test (Mean)	Analytical (i = 6, lower branch)	Frequency Difference (%)
U2U	6,679.66	6,729.00	0.73
T2T	6,716.92	6,729.00	0.18
Acc	6,675.03	6,729.00	0.80
O2O	6,724.51	6,729.00	0.07

The remarkable correspondence of the analytical and experimental frequencies shows that the theory is most appropriate, and the floats are almost perfectly spherical. We cannot predict an understanding of the variability caused by the four sources investigated here (U2U, T2T, Acc, and O2O) using the analytical approach, because these sources of variability are tied to the experimental procedure used to extract the modal frequencies. However, we have demonstrated that these sources of experimental variability result in a variation of features, such as the resonant frequencies, which can be one order of magnitude greater than the test-analysis differences obtained when an idealized theory is used to predict the frequencies of perfect spheres. This result suggests that it makes no sense to "tune" or adjust the predictions of a model beyond the level of variability that can be expected, should the tests be repeated.

Other variability exists that we can examine using the analytical equations, namely, frequency variation caused by small changes in the geometric and material properties of the floats. For the present analysis, we used average values of these parameters, because we restricted our investigation into the variability of marine floats to experimental factors. Future work will address the analytical variations.

7.   Conclusion

The purpose of this report is to examine the sources of variability in a series of modal tests performed on a population of spherical floats. We focused on four areas of variability: the variation in the float itself (U2U), the variation caused by using different operators to perform the test (O2O), the variation in the test setup (T2T), and the variability caused by placing the accelerometers in slightly different positions on the sphere (Acc).

We used a collection of tools to try to assess the amount of variability caused by each of these sources. Almost all methods result in the following conclusions: U2U variability is the largest by a significant margin; second largest is the variability caused by Acc. This variation should be larger than that caused by the T2T repetition, because the same procedure used in the T2T measurements is performed to move the accelerometers to different positions. Thus, Acc encompasses two sources of variability. Most methods find this intuition to be true, with O2O variability contributing about the same as T2T variability.

The methods we used to assess variability in the data that reach the above conclusions include the following: measurement of the correlation between the individual time and frequency responses (Section 5.3.1), the temporal and spectral moments (Section 5.3.2), the first principal component of the time response (Section 5.3.3), and the variation of the frequency values for the first four modes (Sections 5.4 and 6.3). Small deviations occurred in the first principal component of the frequency response, which shows that the Acc variability is only slightly less than the T2T variability, and in the fourth mode, which shows the Acc to be more significant than the choice of float unit. These exceptions are not significant and lead us to believe that we have made a robust assessment of the major contributors to the variation in the modal-response data.

The largest deviation from our main conclusions comes in the modeling of the time response of the system using ARMAX models (Section 5.3.4). The variability of the model-fitting error shows O2O variability to be the largest. An investigation of the variation of the model coefficients shows inconsistent results, with the relative variations changing based on the number of coefficients used in the model. Even though we have no evidence to verify this hypothesis, we suspect that noise in the data and choice of model order are the dominant factors in preventing the forming of an accurate time model.

8. References

1. R. L. Mayes, D. B. Clauss, and J. D. Gruda, "Experimental Characterization of Unit-to-Unit Variability for Components in Payload Systems," in *Proceedings of the 20th International Modal Analysis Conference* (Los Angeles, California, February 4–7, 2002), pp. 679–682.

2. S. W. Doebling, A. Robertson, R. Dolin, J. Pepin, J. Schultze, T. J. Ross, E. Rodriguez, C. Treml, and N. Shah, "Quantifying and Incorporating Parametric Uncertainty for the Prediction of the Nonlinear Crush Behavior of a Population of Steel Marine Floats," Los Alamos National Laboratory Report LA-MS-13983 (March 2002).

3. J. E. Pepin, B. H. Thacker, E. A. Rodriguez, and D. S. Riha, "A Probabilistic Analysis of a Nonlinear Structure Using Random Fields to Quantify Geometric Shape Uncertainties," in *Proceedings of the 43rd AIAA/ASME/ASCE/ASH Structures, Structural Dynamics, and Materials Conference* (Denver, Colorado, April 22–25, 2002).

4. Quality Float Works, 1382 Payne Road, Schaumburg, IL 60173, (847) 781-8960.

5. D. O. Smallwood, "Characterizing Transient Vibrations Using Band Limited Moments," in *Proceedings of the 60th Shock and* Vibration *Symposium* (hosted by the David Taylor Research Center, Underwater Explosions Research Division, Portsmouth, Virginia, November 1989) Vol. III, pp. 93–112.

6. W. R. Dillon, M. Goldstein, *Multivariate Analysis: Methods and Applications* (John Wiley & Sons, New York City, New York, 1984).

7. The Mathworks, Inc., System *Identification Toolbox*, Natick, MA, 2001.

8. J. N. Juang, *Applied* System *Identification* (Prentice Hall, Englewood Cliffs, New Jersey, 1994).

9. W. E. Baker, "Axisymmetric Modes of Vibration of Thin Spherical Shell," *J. Acoustics Society of America* **33**, 1749–1758 (1961).

10. J. P. Wilkinson, "Natural Frequencies of Closed Spherical Shells," *J. Acoustics Society of America* **38**, 367–368 (1965).

Appendix A: Data-Acquisition Setup

Some of the Dactron data-acquisition settings for data collection are listed below, while a picture of the laptop connected to the Dactron system is shown in Figure 45.

- *Engineering units:* Displacement = inch; Velocity = inch/second; Acceleration = g; Force = lbf; Pressure = psi; Voltage = Volt.

- *Time capture:* Enabled for all channels.

- *Spectrum:* Auto-spectra and cross-spectra requested for all measurements.

- *FRF and coherence:* Use the H_2 estimator, $H_2 = G_{ii}/G_{ji}$.

- *Trigger settings:* Analog input; auto arm or manual arm.

- *Averaging:* Type = linear; Domain = frequency.

- *Windowing:* Force exponential.

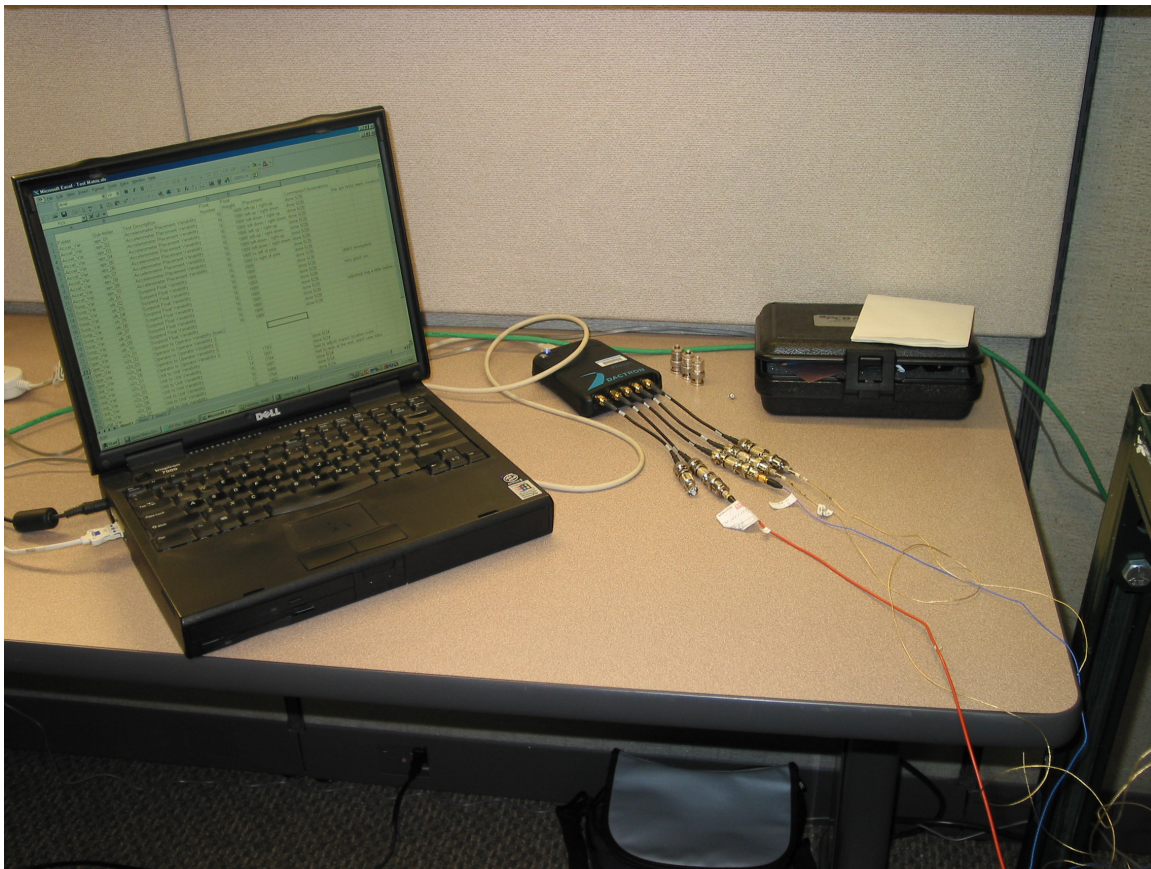**Figure 45: Laptop connected to the Dactron data-acquisition system.**

Appendix B: Data Sets Collected

B-1   Time-Domain and Frequency-Domain Data Sets Collected

Tables 10 and 11 list the type of data collected and stored in the time and frequency domains.

Table 10: Frequency-domain data sets collected.

Coherence	Coh.(2,1); Coh.(3,1); Coh.(4,1)
Auto- and Cross-Spectrum	G(1,1); G(2,1); G(2,2); G(3,1); G(3,3); G(4,1); G(4,4)
Transfer Function	H(2,1); H(3,1); H(4,1)

Table 11: Time-domain data sets collected.

Transfer Function	h(2,1); h(3,1); h(4,1)
Time History for Each Channel	Input(1); Response(2); Response(3); Response(4)

B-2   Data Reference Tables

The measurements collected at each channel of the data-acquisition system are defined below:

- ***Channel 1:***   Impact hammer.
- ***Channel 2:***   Accelerometer, placed on the pole near the weld.
- ***Channel 3:***   Accelerometer, placed on the equator (left side).
- ***Channel 4:***   Accelerometer, placed on the equator (right side).

The data sets collected are stored in separate subfolders, one for each test performed. Each subfolder contains all the measurements (defined in Tables 10 and 11) saved for that particular experiment. The MATLAB[TM] data files in the main (top-level) folder contain the data sets for all experiments in that folder. The MATLAB[TM] data files in each subfolder contain the data sets for that particular test only. Tables 12 and 13 define the type of variability study, the floats used, and where the corresponding data sets are stored.

Table 12: U2U variability data sets and float masses.

Folder	Subfolder	MATLAB^{TM} Data File	Test Type	Float Number	Float Weight [g]
U2U_Variability		U2Udata.mat	U2U Variability (All Data)		
U2U_Variability	u2u_01	U2U1data.mat	U2U Variability	11	1,783.0
U2U_Variability	u2u_02	U2U2data.mat	U2U Variability	12	1,891.0
U2U_Variability	u2u_03	U2U3data.mat	U2U Variability	14	1,794.0
U2U_Variability	u2u_04	U2U4data.mat	U2U Variability	15	1,897.0
U2U_Variability	u2u_05	U2U5data.mat	U2U Variability	16	1,889.0
U2U_Variability	u2u_06	U2U6data.mat	U2U Variability	17	1,784.0
U2U_Variability	u2u_07	U2U7data.mat	U2U Variability	18	1,902.0
U2U_Variability	u2u_08	U2U8data.mat	U2U Variability	19	1,880.0
U2U_Variability	u2u_09	U2U9data.mat	U2U Variability	20	1,789.0
U2U_Variability	u2u_10	U2U10data.mat	U2U Variability	23	1,895.0
U2U_Variability	u2u_11	U2U11data.mat	U2U Variability	25	1,873.0
U2U_Variability	u2u_12	U2U12data.mat	U2U Variability	27	1,905.0
U2U_Variability	u2u_13	U2U13data.mat	U2U Variability	28	1,789.0
U2U_Variability	u2u_14	U2U14data.mat	U2U Variability	29	1,922.0

Table 13: Suspension system and O2O variability tests.

Folder	Subfolder	MATLAB^{TM} Data File	Test Type	Float Number	Float Weight [g]
Suspension_System_Variability		T2Tdata.mat	Suspension Variability (All Data)		
Suspension_System_Variability	sfv_01	T2T1data.mat	Suspension Variability	16	1,889.0
Suspension_System_Variability	sfv_02	T2T2data.mat	Suspension Variability	16	1,889.0
Suspension_System_Variability	sfv_03	T2T3data.mat	Suspension Variability	16	1,889.0
Suspension_System_Variability	sfv_04	T2T4data.mat	Suspension Variability	16	1,889.0
Suspension_System_Variability	sfv_05	T2T5data.mat	Suspension Variability	16	1,889.0
Suspension_System_Variability	sfv_06	T2T6data.mat	Suspension Variability	16	1,889.0
Suspension_System_Variability	sfv_07	T2T7data.mat	Suspension Variability	16	1,889.0
Suspension_System_Variability	sfv_08	T2T8data.mat	Suspension Variability	16	1,889.0
Suspension_System_Variability	sfv_09	T2T9data.mat	Suspension Variability	16	1,889.0
Suspension_System_Variability	sfv_10	T2T10data.mat	Suspension Variability	16	1,889.0
O2O_Variability		O2Odata.mat	Operator to Operator Variability		
O2O_Variability	o2o_01	O2O1data.mat	O2O Variability (IS)	16	1,889.0
O2O_Variability	o2o_02	O2O2data.mat	O2O Variability (TF)	16	1,889.0
O2O_Variability	o2o_03	O2O3data.mat	O2O Variability (NL)	16	1,889.0
O2O_Variability	o2o_04	O2O4data.mat	O2O Variability (FH)	16	1,889.0

(Operators: IS = Isaac Salazar; TF: Tim Fasel; NL: Nathan Limback; FH: François Hemez.)

We conducted the Acc variability tests (Table 14) by placing the equatorial accelerometers slightly off the indicated mark, either up or down. Placement is indicated in the placement column. For example, "Ch. 3-up / Ch. 4-up" means that Channel 3 is slightly moved up from the indicated mark, and Channel 4 is also slightly up moved from the indicated mark. The accelerometers are still in contact with the equatorial weld during this test.

We conducted the high-bandwidth tests (Table 15) to analyze the high-frequency modes of the system. Noise tests (Table 15) were performed with the Channel 2 accelerometer on an arbitrary point on the float, the Channel 3 accelerometer halfway up the yellow leg, and the Channel 4 accelerometer on the upper square tube near the eyelet.

Table 14: Acc variability tests.

Folder	Subfolder	MATLAB™ Data File	Test Description	Placement
Accel_Placement_Variability		Adata.mat	Acc Variability (All Data)	
Accel_Placement_Variability	apv_01	A1data.mat	Acc Variability	Ch. 3-up/Ch. 4-up
Accel_Placement_Variability	apv_02	A2data.mat	Acc Variability	Ch. 3-up/Ch. 4-down
Accel_Placement_Variability	apv_03	A3data.mat	Acc Variability	Ch. 3-down/Ch. 4-up
Accel_Placement_Variability	apv_04	A4data.mat	Acc Variability	Ch. 3-down/Ch. 4-down
Accel_Placement_Variability	apv_05	A5data.mat	Acc Variability	Ch. 3-up/Ch. 4-up
Accel_Placement_Variability	apv_06	A6data.mat	Acc Variability	Ch. 3-up/Ch. 4-down
Accel_Placement_Variability	apv_07	A7data.mat	Acc Variability	Ch. 3-down/Ch. 4-up
Accel_Placement_Variability	apv_08	A8data.mat	Acc Variability	Ch. 3-down/Ch. 4-down
Accel_Placement_Variability	apv_09	A9data.mat	Acc Variability	Ch. 2 on left side of pole
Accel_Placement_Variability	apv_10	A10data.mat	Acc Variability	Ch. 2 on right side of pole

Table 15: High-bandwidth and noise tests.

Folder	Subfolder	MATLAB™ Data File	Test Description	Float Number	Float Weight [g]
U2U_Variability_Hi_Bandwidth		Bdata.mat	High-Bandwidth Test (All Data)		
U2U_Variability_Hi_Bandwidth	run_01	B1data.mat	High-Bandwidth Test	16	1,889.0
U2U_Variability_Hi_Bandwidth	run_02	B2data.mat	High-Bandwidth Test	17	1,784.0
U2U_Variability_Hi_Bandwidth	run_03	B3data.mat	High-Bandwidth Test	18	1,902.0
U2U_Variability_Hi_Bandwidth	run_04	B4data.mat	High-Bandwidth Test	19	1,880.0
U2U_Variability_Hi_Bandwidth	run_05	B5data.mat	High-Bandwidth Test	20	1,789.0
Noise		Ndata.mat	Noise Tests (All Data)		
Noise	noise_01	N1data.mat	Background noise	16	1,889.0
Noise	noise_02	N2data.mat	Effect of impact on yellow leg	16	1,889.0
Noise	noise_03	N3data.mat	Effect of impact on green leg	16	1,889.0
Noise	noise_04	N4data.mat	Free run (stomping on ground)	16	1,889.0
Noise	noise_05	N5data.mat	Free run (no stomping)	16	1,889.0

Appendix C: Impulse- and Frequency-Response Functions

C-1 Impulse-Response Function

The dynamic properties of linear, time-invariant systems can be described by the impulse-response function, *h(t)*, which is defined as the output of a system to a unit impulse input. The impulse-response function is obtained for any arbitrary input *u(t)* through the convolution integral:

$$y(t) = \int_{-\infty}^{\infty} h(\tau)u(t-\tau)d\tau \tag{11}$$

where *y(t)* is the response of the system to the arbitrary input *u(t)*, and *τ* is a time-translation parameter used to perform the convolution.

C-2 Frequency-Response Function

The frequency-response function *H(f)* can be found directly from the impulse-response function by taking its Fourier transform:

$$H(f) = \int_{-\infty}^{\infty} h(t)e^{-j2\pi ft}dt \tag{12}$$

More often, however, the frequency-response function is constructed from the auto-spectral and cross-spectral density functions of the input and output data:

$$H(f) = \frac{Gyu}{Guu} \tag{13}$$

The cross-spectral density function G_{yu} of the input and output data is defined as:

$$Gyu(f) = Y(f)U^*(f) \tag{14}$$

where *Y(f)* denotes the Fourier transform of the output, and *U*(f)* is the complex conjugate of the Fourier transform of the input. Similarly, the auto-spectral density function G_{uu} is defined as:

$$Guu(f) = U(f)U^*(f) \tag{15}$$

Appendix D: Material and Geometric Properties

Material and geometric properties (English units):

- ***Modulus of elasticity:*** 28.00 x 10^{+8} psi.
- ***Density:*** 7.51 x 10^{-4} slug-in.
- ***Poisson's ratio:*** 0.28.
- ***Mid-surface radius:*** 4.4688 in.
- ***Thickness:*** 0.0625 in.

Material and geometric properties (SI units):

- ***Modulus of elasticity:*** 1.931 x 10^{+11} Pa.
- ***Density:*** 8.026 x 10^{+3} kg/m^3.
- ***Poisson's ratio:*** 0.28.
- ***Midsurface radius:*** 113.51 x 10^{-3} m.
- ***Thickness:*** 1.588 x 10^{-3} m.